Adaptive Neural Networks Control for Unknown Flexible Joint Robots and Piezoelectric Actuators

Han YAO

A Thesis

in

The Department

of

Mechanical and Industrial Engineering

Presented in Partial Fulfillment of the Requirements

For the Degree of Master of Applied Science at

Concordia University

Montreal, Quebec, Canada

August 2006

Your file Votre référence
ISBN: 978-0-494-30080-0
Our file Notre référence
ISBN: 978-0-494-30080-0

ABSTRACT

Adaptive Neural Networks Control for Unknown Flexible Joint Robots and Piezoelectric Actuators

Han YAO

In the thesis, motivated by the well-known universal approximation capability (input-output mapping) of the neural network (NNs), we have proposed adaptive NN controllers for a Rigid Link Flexible Joint (RLFJ) robot manipulator with unknown nonlinearities and piezoelectric actuator with unknown hysteresis, respectively.

For a RLFJ robot manipulator, the dynamic model is decomposed into two different time scale models by using integral manifold method. The control torque consists of two terms: slow and fast terms for two time scale models. A composite NN-based control strategy is proposed for the position and velocity tracking of the manipulator. Two multilayer NNs are used to approximate two unknown nonlinear functions. These two NNs are tuned on-line without any off-line training. The stabilities of composite control system have been proved. The boundedness of NN weights and control signal of systems are guaranteed. Simulation results verify the developed control algorithms.

The feedforward multilayer NN is also further investigated to approach the complicated nonlinear function in proposed hysteresis dynamics, which is described by Duhem model. An adaptive NN compensator is designed for unknown hysteresis in a piezoelectric actuator. A pre-inverse hysteresis function is well-structured and the effect of the actuator hysteresis is cancelled. The simulation results are also presented to show the effectiveness of the developed adaptive control scheme.

Acknowledgements

I wish to express my profound thanks to my supervisor, Dr. W. F. Xie, for her invaluable guidance at every stage of this thesis. Her broad knowledge on control area encourages me to study deeply in this research field.

I am also very grateful to my classmates and friends for their helps and advices during my research.

Finally, I would like to express my special thank my parents, for their encouragement, support and help in my study and life.

Han YAO

Montreal, Canada

Table of Contents

List of Figures

List of Tables

List of Symbols, Abbreviations and Nomenclature

Symbol	Definition
NN	Neural Network
MLP	Multilayer perceptron
RLFJ	Rigid Link Flexible Joint
RLRJ	Rigid Link Rigid Joint
SMAs	Shape Memory Alloys
τ_{pd}	The Desired Control Signal of Piezoelectric Actuator
τ_{pr}	The real Control Signal of Piezoelectric Actuator
e_p	The Residue Error of Piezoelectric Actuator
c	The Constant Slop of Piezoelectric Actuator Control Signal
d_p	The Disturbance of Piezoelectric Actuator Control Signal Caused by the Hysteresis
$tr(\cdot)$	The Trace
$\|\cdot\|_F^2$	The Frobenius Norm
$\sigma(\cdot)$	The Transfer Function of the Neuron
V^T	The Weight Matrix of hidden layer of NN
W^T	The Weight Matrix of output layer of NN

$\varepsilon(x)$	The Functional Restructure Error Vector
$\gamma_{\beta,\alpha}[u \quad \zeta](t)$	The Preisach Hysteresis Operator
P_0	The Preisach plane
$\mu(\beta, \quad \alpha)$	The Weight Function of Preisach Hysteresis
K_L	The Kinetic Energy
P	The Potential Energy
q	The Joint Variables of the Robot Manipulator
τ	The Control Torque of the Robot Manipulator
$M(q)$	The Inertia Matrix
$V(q,\dot{q})$	The Coriolis and Centripetal Vector
$G(q)$	The Gravity Vector
$F(\dot{q})$	The Friction Vector
T_L	The Disturbance Vector
σ_0	The Stiffness Coefficient of Friction
σ_1	The damping Coefficient of Friction
σ_2	The Viscous Friction Term
J	The Motor Inertia Coefficient of RLFJ
B	The Joint Damping Term of RLFJ
K	The Stiffness Coefficients Matrix of RLFJ
q_f	The Motor Shaft Variables of the Robot Manipulator
γ	The Inverse of Stiffness Coefficient

$q_d(t)$	The given desired trajectory of the Robot Manipulator
$e(t)$	The Tracking Error of the Robot Manipulator
$r(t)$	The Filtered Error of the Robot Manipulator
τ_s	The Control Torque of the Robot Manipulator Slow Part
τ_f	The Control Torque of the Robot Manipulator Fast Part
z	The Difference Between the Link and Motor Position
τ_0	The Control Torque to the Rigid Robot Manipulator
τ_1	The Corrective Torque Term of the Robot Manipulator
K_v	A Gain Matrix for the Control Torque
$\lambda_{v\min}$	The Minimum Eigenvalue of Gain Matrix K_v
L_1	The Lyapunov function for the Rigid Robot Manipulator
φ	The Fictitious Variable of the Robot Manipulator
K_u	A Gain Matrix for the Fictitious Variable
K_f	A Gain Matrix for the Joint Elasticity
L_2	The Lyapunov Function for the RLFJ
$H(t)$	The Hysteresis Function
$g(v)$	The Slope of the Duhem Model
$f(v)$	The Average Different Value of the Duhem Model
$v(t)$	The Input of the Duhem Model
χ_k	The Indicator Function

$HI(t)$	The Inverse Hysteresis Function
$\widetilde{\tau}_{pr}$	The Error Between the Desired Control Signal and Real Control Signal of Piezoelectric Actuator
τ_{p0}	The initial control signal value of Piezoelectric Actuator
c_k	The Jump Point of a Piecewise Nonlinear Function
$\hat{\mu}$	An Estimated Constant of Piezoelectric Actuator
$\Pr oj(\cdot)$	A Projection Operator
$e_p(t)$	The Tracking Error of the Piezoelectric Actuator
$r_p(t)$	The Filtered Error of the Piezoelectric Actuator
Y_d	The Input Signal of the Piezoelectric Actuator
k_{pd}	A Gain Matrix for the Piezoelectric Actuator
k_b	A Gain Matrix for the Hysteresis Compensation
L_3	The Lyapunov Function for the Piezoelectric Actuator

Chapter 1 Introduction

1.1 Motivation

Over the last decade, interest in the control of robot manipulators has increased significantly, since they are commonly used in the manufacturing industry such as painting, welding and material handling in the manufacturing industry. In order to increase the productivity and meet the high tolerance requirement, it is essential for the manipulators to follow the desired trajectories as close as possible at the fast operational speed. Many control strategies have been developed for the control of robot manipulators, such as exact compensation of nonlinearities, robust adaptive algorithms, variable structure theory etc. [1]-[4]. These control methods share the common feature that the robot dynamics are modeled by the rigid link rigid joint (RLRJ) equations of motion. Unfortunately, experimental evidence indicates that the assumption of perfect rigidity is never satisfied exactly in the real world. As a result, those control strategies, which is designed for RLRJ robot manipulators, is inadequate for the RLFJ robot manipulators. The flexibility limits the system performance and introduce undesirable inaccuracies or oscillations. In some cases, joint flexibility can even lead to instability if it is neglected in the control design.

To deal with these problems, a number of control schemes based on the flexible models have been developed to control flexible-joint robots. These methods include feedback linearization [5, 6], singular perturbation techniques [7], sliding mode [8], and robust adaptive controller approaches [9, 10]. However, these existing control schemes have some drawbacks such as the complexity in deriving the expression of the control

signal and the computational cost of implementation.

On the other hand, several smart material-based actuators have been widely utilized in today's manufacturing industrial system like robot manipulator. Those smart actuators fit well for micro-positioning devices in precision manufacturing engineering because of their fast response, low-order and stronger driving force. However, hysteresis is common in all these actuators, such as piezoceramics and shape memory alloys (SMAs). It deteriorates both static and dynamic performance of systems, sometimes, even leading to oscillation and instability. Therefore, designing control methods to compensate for the hysteresis nonlinearity associated with piezoelectric actuator plays an important role in the construction of these smart structures.

Recently, many NN controllers with closed-loop stability [11, 12, 13, 14] have been proposed for various control applications, due to its ability of universal function approximation. In the thesis, NN based controllers are developed for both controlling of a RLFJ robot manipulator and compensating the hysteresis in piezoelectric actuators.

1.2 Literature review

1.2.1 Control strategies for RLFJ robot manipulator

More and more robot manipulators in today's industry use compact Harmonic driver as joint. It is used to replace the heavy and bulky drives because it can achieve better mechanical structures, improve mobility, and offer the same gear ratios with much smaller gear sizes [15,16]. All those advantages come from the utility of the non-rigid flexible spine, which naturally results in increased flexibility at the robot joints. As a result, robots with harmonic drivers will exhibit significant joint flexibility.

Actually, experimental and simulation studies on industrial robot manipulators showed that these are two different flexibilities exist in robot manipulators: link flexibility and joint flexibility [17, 18, 19, 20]. Both of them have a significant influence on robot dynamics. Link flexibility, which refers to the elastic links, results in a deflection of the link. Joint flexibility, which refers to the elastic joints, results in a difference between the joint angle and the actuator shaft angle. Since link flexibility depends on the link stiffness and length, it can be suppressed by increasing the links' cross-sectional moments of inertia. On the contrary, joint flexibility cannot be compensated as easily as link flexibility. As a result, the performance of a robot manipulator depends on this control system to suppress the joint flexibility [21]. That is the reason why, in real applications, robot manipulators always be treated as rigid-links interconnected by elastic joints. Thus, the joint flexibility should be taken into account in both modeling and control designing if high performance is to be achieved.

From the modeling point of view, flexibility introduces fast dynamics and additional degrees of freedom. The motor shaft angle is no longer equivalent to the link angle and the order of the related dynamics becomes twice that of rigid robots. A more complicated mathematical model is needed to describe the behaviour of the RLFL robot manipulator [22,23].

On the other hand, from the control designing point of view, those control schemes for rigid robots, such as exact compensation of nonlinearities, robust adaptive algorithms, variable structure theory, need to be adjusted for the high performance when the joint flexibility is taken into account [24,25]. The control problems of flexible joint robots are more challenging if uncertainties such as unknown payload variations and external

disturbances, unknown parameters in the system dynamics, are considered. Many researches have focused on the control of flexible-joint robot manipulators such as feedback linearization, singular perturbation, backstepping based control scheme, and Neural Network based control strategies.

Feedback linearization

Feedback linearization is a well-known control approach for nonlinear systems. Usually, it consists of two parts: nonlinear feedback terms to cancel the nonlinearities and a designed control strategy for the equivalent linear closed-loop system. Feedback linearization [3, 4, 17] is widely used to design the controller for rigid robot manipulator.

A feedback linearization approach [3] is used to calculate the computed torque control signal and work as an inverse dynamics as shown Figure 1-1. The unknown dynamic nonlinearities in the manipulator model such as load, link mass parameters, and friction parameters are estimated on-line. A globally stable adaptive control scheme is designed with the computed torque.

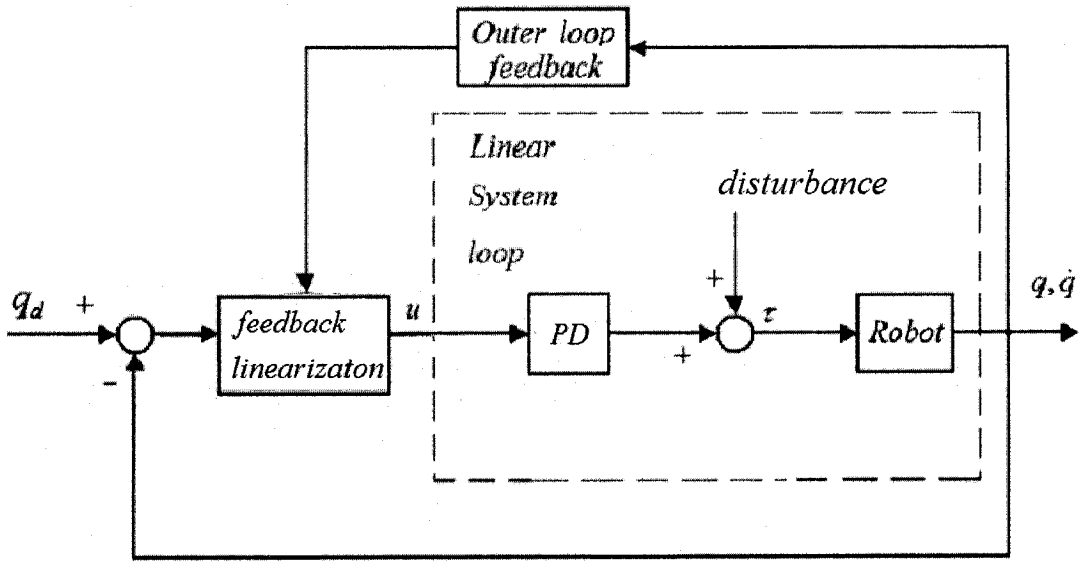

Figure 1-1 Computed-torque control scheme

In feedback linearization, the position, velocity and acceleration of both links and joints need to be measured due to the exact cancellation for the system nonlinearities need to be measured. Moreover, the full knowledge of robot manipulator dynamic is needed and it's unrealistic for the precise knowledge of all the states. An asymptotic observer [2] is designed based on only the position measurement of both link and joint to estimate the joint speed. The convergence of a trajectory is ensured when the nonlinear observer gain constant satisfies the suitable inequalities. However, the design of the nonlinear observer is very complicated and easily subject to the disturbance.

In summary, feedback linearization algorithm is an option for rigid or flexible robot manipulator control. The control performance depends on the knowledge of system dynamics and states. For a precise tracking trajectory, an observer is required to estimate the unknown system parameters and states.

Singular perturbation

Usually, the joint stiffness is large comparing with other parameters in a flexible joint robot manipulator. Therefore, most singular perturbation control schemes are designed under the assumption of weak flexibility. As a result, the robot manipulator dynamics can be decomposed into two different time scale models: fast subsystem and slow subsystem by using the singular perturbation algorithm. Then a corrective term is plugged into the control law for slow subsystem (rigid robot manipulator) to compensate the fast subsystem (joint elasticity). The singular perturbation algorithm is widely used for the control strategy of the flexible joint robot manipulators.

In the category of singular perturbation techniques, the integral manifold scheme in the context of composite control has been investigated [21, 24, 25]. The integral manifold is a tool for reducing the order of the model, for example a 2n-order system dynamics can be described by an n-order mathematical model. The approaches start with strategies dealing with the flexible joint robot with known parameters and are later on extended to the integration of composite control and corrective control methods to cope with flexible joint robot with unknown parameters—so called "adaptive integral manifold" approach. Research efforts have been focused on dealing with the effects of un-modeled dynamics and system parameter variations using the reduced order model of the flexible-joint manipulators. Although the reduced order model has the same order as the rigid robot manipulator, the effects from flexible joints have already been considered in the model.

The concepts of feedback linearization, singular perturbation, integral manifold and composite control have all been used for adaptive control of flexible joint robot manipulator [24]. A corrected slow subsystem is augmented by a dynamical controller to

ensure an asymptotic tracking capability. With the corrective term, the close loop dynamics of system become a linear system dynamics. The tracking problem becomes tracking the slow output and stabilizing the corrected fast subsystem by using dynamic output feedback. The major advantage of the proposed strategy is that the only measurements required are tip positions, joint positions, and joint velocities. The new strategy allows for smaller tip position tracking errors and its implementation does not require any measurement of change rates of deflection variables with time. However, the control law is too complicated to implement in the real-time control. Thus, the symbolic manipulation software and fast real-time control technology is indispensable.

The algorithm includes the rigid control scheme for slow subsystem and a corrective term for fast subsystem. It is also known as composite control algorithm because it consists of two different control systems. A simple correction term is added to the control law to damp out the elastic oscillations at the joints [25]. In this way, the fundamental properties of rigid robot dynamics may be exploited to design adaptive control laws for flexible joint robots that are robust to parametric uncertainty. The advantages of composite control scheme are: first, the scheme is roughly the same as rigid adaptive control scheme; second, the implementation of the controller needs only position and velocity of joint, the acceleration and jerk measurements are unnecessary.

More recently, the singular perturbation method and the sliding mode control techniques are combined to achieve classical control objectives for nonlinear flexible joint robot manipulators with parametric uncertainties [26]. An observer is designed for estimating the immeasurable components of the vector state of the controll law. Furthermore, the observer-control scheme is applied to a model of a permanent magnet

stepper motor for regulating the angular position.

In summary, the approach using integral manifold approach can reduce the order of the flexible robot manipulator dynamics by decomposing the system model into fast subsystem and slow subsystem. With the compensation of a corrective term for fast subsystem, those conventional control strategies for rigid system can be used in the flexible case. No acceleration and jerk measurements are needed. That is the reason why this thesis follows the same idea. The seeming drawbacks of the traditional integral manifold method are its complexity in deriving the expression of the slow control and the computational cost of implementation. These problems are more pronounced in the adaptive integral manifold method [7]. Although the current advances in symbolic software and parallel computing technologies have facilitated the computationally intensive control algorithm, the symbolic computation remains intractable as it hinges on the robot's nonlinear model that is hard to be identified and verified. Moreover, the symbolic computation of symbolic has to be carried out again whenever the RJFL robot is changed.

Backstepping based control scheme

The backstepping technique starts from a known state space dynamics $\dot{x} = f(x,u)$. A series of fictitious inputs signals ξ_1, $\xi_2,\ldots,\xi_k$ are defined to create series of new dynamics $\dot{x} = f(x,\xi_1)$, $\dot{\xi}_1 = \xi_2$, $\dot{\xi}_2 = \xi_3, \ldots, \dot{\xi}_k = u$. Thus, the original system is described by a chain of integrators. With the knowledge of global asymptotical stability of the error equation $\dot{x} = f(x,\xi_1)$, a series of error terms are defined and a series of integrators are added into their input. As the result, a new feedback law for the

augmented system is developed and global asymptotical stability of system is guaranteed. Recently, backstepping technique is used for developing the control scheme of the flexible joint robot manipulators.

A backstepping control scheme is presented for flexible joint robot manipulators, and asymptotic stability is ensured regardless of the joint flexibility value, which means the results are not restricted to weak joint elasticity [18]. The control input is computed using link and motor shaft position and velocity measurements. Joint position and velocity tracking errors converge to zero with all the signals in the system remaining bounded. However, the approach needs the inverse inertia matrix of the robot manipulator to eliminate the link acceleration measurement. Therefore, the complicated control law is needed to calculate the inertia matrix.

In summary, the backstepping based control strategy can be used to design the controller for flexible joint robot manipulators without any restriction on the magnitude of the joint flexibility or the need for acceleration measurements. The globally asymptotically stable position tracking is guaranteed. No prior system knowledge is needed. The seeming drawbacks of the backstepping based control strategy are: first, complicated control law is indispensable and the computation burden is intensive; second, persistent excitation of input signal for parameter adaptation is needed. These issues still need to be analyzed for the further utility of this approach in flexible joint robot manipulator.

Neural Network based control strategies

With the universal approximation property and learning capability [27], NNs have

been proved a powerful tool to control complex nonlinear systems with parameter uncertainties such as RLFJ robot manipulator. Many researches have proposed to design various NN based control schemes for the RLFJ robot manipulator.

With different structures, NNs can be decomposed into two types: feedforward and recurrent. Both of them can be used in direct control for the RLFJ robot manipulator. Recently, many NN controllers with closed-loop stability [11, 12, 13, 14] have been proposed for various control applications. Due to its ability of universal function approximation, NN has been successfully used to design controllers for RLFJ robot manipulators [8, 28, 29]. Not like the traditional control strategies, NN based controller does not need the completely formulated mathematical model, which usually is unavailable or complicated.

NNs can be used to approximate the inverse nonlinear function to compensate the flexible nonlinearities [8, 28]. In the above work, off-line training is used to obtain the preliminary weights. Kwan et al. [11] proposed a robust NN backstepping control method shown as Figure 1-2 for nonlinear systems and applied it to RLFJ robots without weak elasticity assumptions. The NNs are used to approximate two very complicated nonlinear functions. The controller does not require either a linear parametrizable model or an off-line learning phase. The persistent excitation condition of certain signals is not necessary either.

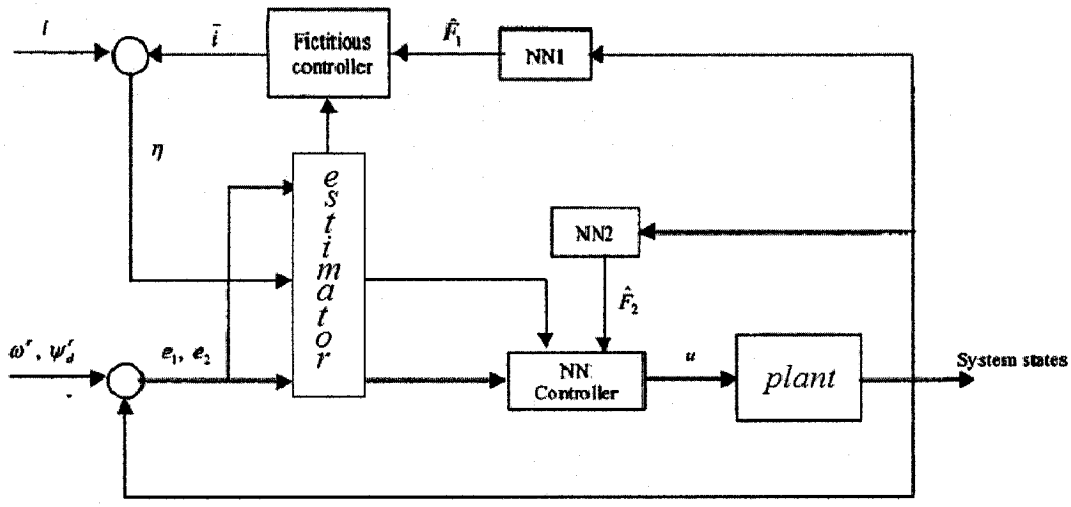

Figure 1-2 NN controller structure [11]

A recurrent NN approach is presented for the motion control of constrained flexible manipulators [30]. The developed control scheme can adaptively estimate the underlying dynamics of the manipulator using recurrent NN. Based on the error dynamics of a feedback controller, a learning rule for updating the connection weights of the adaptive recurrent NN model is obtained.

In summary, with the universal approximation property and learning capability, NNs have been proved a powerful tool to control complex nonlinear systems with unknown parameters. It is widely used with adaptive robust control for guaranteed stability of systems. The common usage of NNs is to estimate or approximate unknown nonlinear dynamics. The Lyapunov theory is always used with NN to ensure stability of the entire system, the convergence of the tracking error and boundedness of NN weight matrix.

1.2.2 Hysteresis Dynamic model

In today's industry, the smart actuators are normally used because of their fast response, low-order and stronger driving force. Hysteresis is common in all the smart material-based actuators, such as piezoceramics and shape memory alloys (SMAs). Hysteresis is general nondifferentiable, nonlinear, and unknown nonlinearity. In the other words, a general hysteresis model is difficult to obtain due to its complexity. Many different mathematic models are built to describe the hysteresis behaviour such as: Preisach model, Prandtl-Ishlinkii model, and Duhem model. Those models can be classified into two different groups. The first one is called physics-based such as Jiles-Atherton model [31]. The other one is called phenomenology-based such as Preisach operator [32]. Physics-based model are built on principles of physics, while phenomenology-based model just produce behaviours similar to those dynamics without any physical meaning. This section will give a brief introduction for some of these hysteresis models.

Preisach model

The basic idea of Preisach model is to represent a large class of hysteresis operators as an average of relays [32,33]. For a pair of thresholds (β, α) with $\beta \le \alpha$, consider a simple hysteresis operator $\gamma_{\beta,\alpha}[u \quad \zeta](t)$, which is shown in Figure 1-3. With $\zeta \in \{-1, \quad 1\}$, the function

$$v(t) = \gamma_{\beta,\alpha}[u \quad \zeta](t) = \begin{cases} -1, & u(t) < \beta \\ 1, & u(t) > \alpha \\ v(t^-), & \beta \le u(t) \le \alpha \end{cases} \tag{1.1}$$

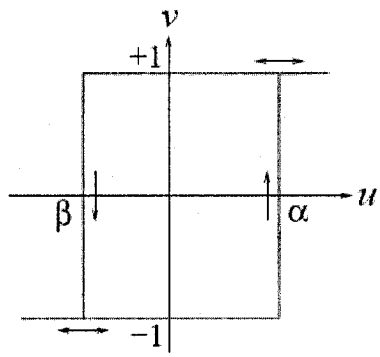

Figure 1-3: Preisach hysteresis model

Although in general the Preisach model does not provide physical insight into the problem, it provides a means of developing phenomenological models that are capable of producing behaviors similar to those of physical systems. For example, magnetostriction phenomenon is a strong coupling between magnetic properties and mechanical properties of some ferromagnetic materials. It is rate-independent when the input frequency is low. Hysteresis, which is exhibited by magnetostrictive actuators, can be modeled by the Preisach operator [32].

Prandtl-Ishlinkii model

The Prandtl-Ishlinkii (PI) model is commonly a rate-independent backlash operator. It can be described as follows [34]

$$\begin{aligned} y(t) &= H_r[x, y_0](t) \\ &= \max\left\{x(t) - r, \quad \min\{x(t) + r, y(t - T)\}\right\} \end{aligned} \tag{1.2}$$

where x is the control input, y is the actuator response, r is the control input

threshold value or magnitude of the backlash, and T is the sampling period. The initial consistency condition of the PI operator is

$$y(0) = \max\left\{x(0) - r, \quad \min\{x(0) + r, y_0\}\right\} \tag{1.3}$$

The PI model is formulated to describe the elastic-plastic behaviour [35]. The elementary operator in the PI hysteresis model is a rate-independent backlash or linear-play operator. The main advantage of PI model is its less complexity. Thus, due to its suitability for real time applications and the existence of a closed form solution for its inverse, it is commonly used in the modeling of backlash between gears with one degree of freedom.

1.2.3 Control strategies for hysteresis

There is an increasing usage of piezoelectric actuators in precision machining due to their fast response, low-order and stronger driving force. An unavoidable nonlinearity of these actuators is hysteresis, which refers to the input-output relation between two time-dependent quantities that cannot be expressed as a single-value function [36]. It is the key factor limiting both static and dynamic performance of the piezoelectric actuators.

Hysteresis is general nondifferentiable, nonlinear, and unknown. In the other words, a general hysteresis model is difficult to obtain because of the complexity of hysteresis phenomenon. The existence of hysteresis will reduce the accuracy, introduce oscillation and even cause the instability to the control system. Thus, it poses a challenge to the controller design. Various approaches are designed to compensate the hysteresis such as inverse hysteresis compensation, hysteresis partition compensation, and direct control

without constructing a hysteresis inverse.

Inverse Hysteresis Compensation

For eliminating the effect of hysteresis, one common method is to build a feedforward inverse hysteresis function, as shown in Figure 1-4

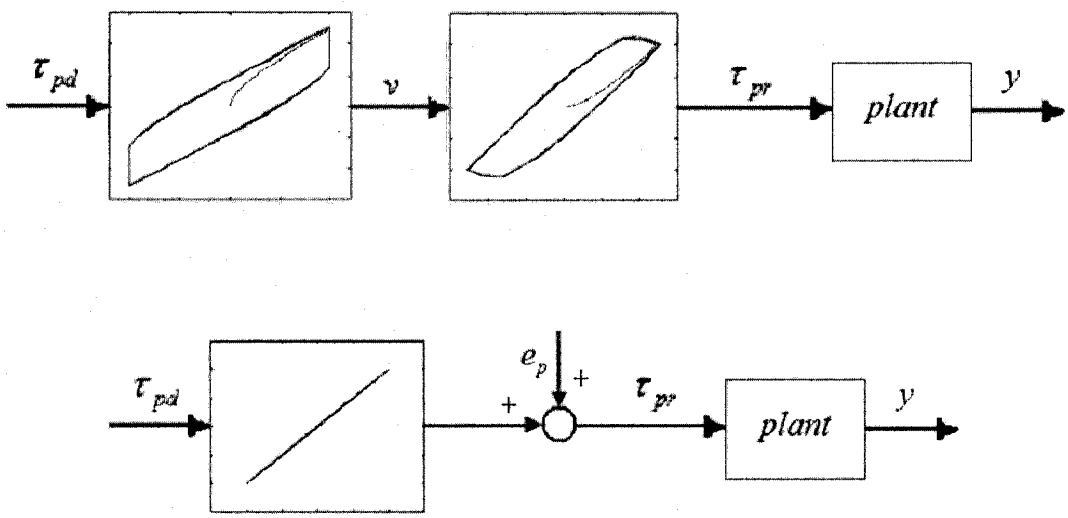

Figure 1-4 Inverse hysteresis compensator

The input control signal can be described as

$$\tau_{pr} = \tau_{pd} + e_p$$

where e_p is the residue error caused by the mismatching of the inverse model.

Based on different hysteresis dynamic model, such as the Duhem model, and the Preisach model, various inverse compensators [32, 37, 38] are designed. A parameterized hysteresis model is presented and an adaptive hysteresis inverse is developed, which is

capable of achieving a linear parameterization [37]. Another proposed controller contains a feedback linearization control with a reference model and a sliding-mode control [38]. A fixed point and closest-match algorithm for approximately inverting the Preisach operator is also presented [32].

NN is also a powerful tool for hysteresis compensation. Feedforward NN models are used to describe the hysteresis behaviour in different frequencies with the knowledge of some properties of magnetic materials, such as loss separation property to allow the separate treatment of quasi-static and dynamic hysteresis effects [39,40]. The proposed feedforward NN models for vector dynamic hysteresis are fast, require no large data set, and apply standard NN algorithms. Taking [41] as another example, a modified Luenberger observer and a NN are used to identify a general model of hysteresis. Then the identification approach provides stable adaptation of the system. A recurrent NN is designed [42] to compensate an unknown hysteresis.

In summary, inverse hysteresis compensation is a fundamental approach to hysteresis. The basic idea of inverse hysteresis compensation is to construct an inverse feedforward hysteresis to remove the effect of hysteresis phenomena. Then, the output approximately approaches to the reference trajectory.

Hysteresis Partition Compensation

Hysteresis can be divided into two parts [43]: linear part and disturbance part as shown in Figure 1-5

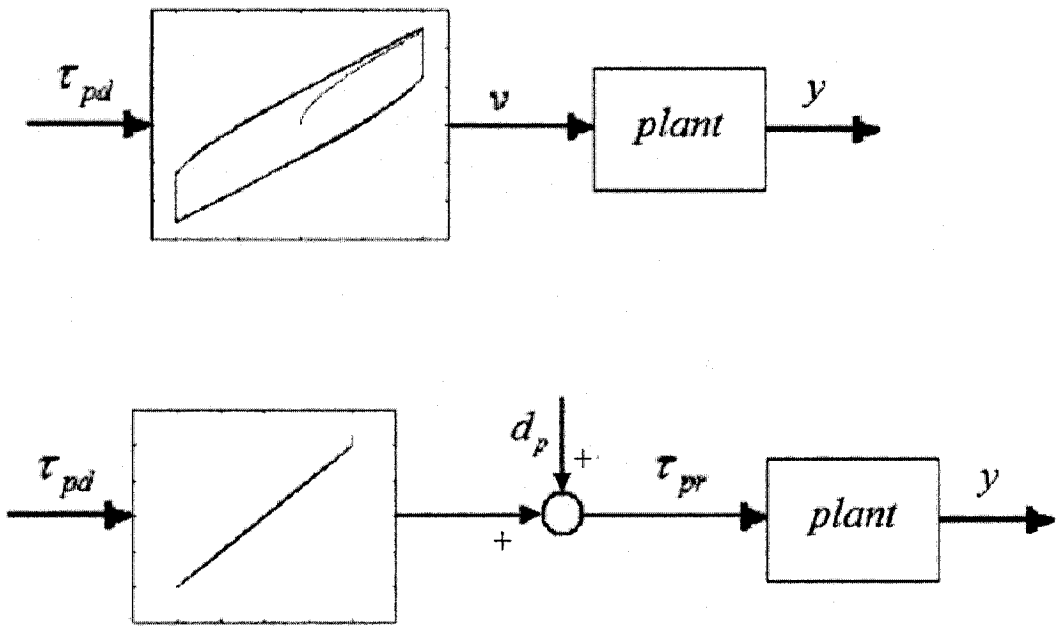

Figure 1-5 Hysteresis partition compensator

The input control signal can be described as

$$\tau_{pr} = c \cdot \tau_{pd} + d_p$$

where c is a constant slop, d_p is the disturbance caused by the hysteresis, which is bounded.

In summary, an observer is usually designed in hysteresis partition compensation to estimate those unknown states such as disturbance of the unknown hysteresis, excitation force, and its derivative. For tracking the reference trajectory, the control scheme contains an adaptive controller, a reference model, and a nonlinear observer. The controller includes two parts: equivalent control and switching control. The equivalent

control is constructed to perform the desired control behavior; the switching control is employed to ameliorate the robust performance.

Direct control without Hysteresis Inverse

In direct control method, a control strategy is designed for the whole system, which is considered by fusing the hysteresis dynamics into the plant dynamics. Based on the solution properties of the differential equation of hysteresis dynamic model, a robust adaptive control algorithm can be developed without constructing a hysteresis inverse [44].

In summary, the adaptive direct control algorithm can deal with a class of nonlinear dynamic systems preceded by unknown hysteresis nonlinearities without constructing a hysteresis inverse. The control law ensures global stability of the entire system and achieves both stabilization and tracking within a desired precision.

1.3 Research objectives and main contributions of this thesis

1.3.1 Research objectives

In this thesis, the robot manipulator is considered as a two-link RLFJ robot manipulator. The dynamic model of the system is derived by Lagrangian formulation. The hysteresis is described by the Duhem model. NN presented in the thesis is feedforward Multilayer perceptron (MLP). The main research objectives of this thesis are:

1) To develop an NN based composite adaptive approach for a RLFJ robot manipulator with unknown nonlinearities.

2) To design an adaptive estimator and a NN to build a dynamic pre-inversion hysteresis compensator to compensate the effect of hysteresis.

3) To design a controller by fusing the hysteresis compensate strategy with the adaptive control scheme for a piezoelectric actuator proceeding with hysteresis

1.3.2 Main contributions

In this research, NN based adaptive control schemes are extensively studied for different nonlinear systems. The main contributions are summarized as:

- Two multilayer NNs is used in each of fast and slow controllers to approximate two explicit nonlinear functions in rigid model and flexible joint model to alleviate the symbolic computational burden.
- For the flexible-joint based component of the fast controller, a fictitious variable is introduced in the design of the fast NN controller to provide sufficient damping for the fast dynamics.
- The hysteresis compensator is designed to reduce the effect of hysteresis by constructing a pre-inverse function. Since the pre-inverse function is constructed without considering the plant dynamics, this compensator can work within many different systems.
- All the NNs in both RLFJ robot manipulator control and piezoelectric actuator with the hysteresis are developed to be tuned on-line without prior offline training.
- All the NNs' weight matrix update rules in both RLFJ robot manipulator control and piezoelectric actuator with the hysteresis are designed using the Lyapunov theorem extension [45] to ensure the system stability. It has been proven that the proposed NN

controller guarantees the boundedness of tracking errors and weight updates.

1.4 Thesis Outline

The thesis is organized as follows:

In Chapter 2 some mathematical preliminaries is introduced. The mechanism and structure of feedforward MLP is given.

In Chapter 3, the development of the adaptive NN based controllers for both rigid and flexible joint robots are detailed and the system stability is proved.

In Chapter 4, the numerical implementation of the RLFJ controller is carried out and the simulation result is given

In Chapter 5, the NN based compensator for hysteresis is designed and combined with an adaptive controller for piezoelectric actuator. The whole system stability is also proved.

In Chapter 6, the numerical implementation of the hysteresis compensator is applied to an adaptive controller for a piezoelectric actuator and the simulation result are given

In Chapter 7, some possible future work and conclusion are given.

1.5 Conclusion

In this chapter, several issues regarding the design and implementation of the NN based adaptive controllers for both RLFJ robot manipulator and piezoelectric actuator with hysteresis are discussed. The motivation of the thesis is provided. An extensive literature review on RLFJ robot manipulator and actuator hysteresis is given. The research objective and contribution are presented in the thesis.

Chapter 2 Mechanism and Structure of Neural Network

Artificial Neural Networks (ANNs) are inspired by the structure and functions of the biological neural networks (BNNs) [46, 47, 48]. ANNs have some capabilities of BNNs, such as storing information, processing information, self-learning, and justification. The NN have been explored to approximate any function with arbitrary degree of accuracy [49]. It can be trained to solve problem such as complex function approximation, pattern recognition, classification and identification.

Neural networks can be categorized into two major types: feedforward networks and recurrent networks. Although recurrent NNs have demonstrated strong nonlinear characteristics in a large amount of research works, they suffer from the lengthy training processes, which are not suitable for real-time control implementation. In the literature, feedforward NNs are most popularly used for nonlinear system identification. A typical example is the MLP, which is utilized to identify the dynamic characteristics of a nonlinear system. The main characteristic of MLP—fast convergence makes it prime candidate for adaptive control of nonlinear systems. In this Section, the mechanism and structure of MLP are introduced. We also investigate the augmented MLP for approximating the piecewise continuous function.

2.1 Mathematical Preliminaries

Given $A = \lfloor a_{ij} \rfloor$, $B \in R^{m \times n}$ the Frobenius norm is defined by

$$\|A\|_F^2 = tr(A^T \cdot A) = \sum_{ij} a_{ij}^2 \tag{2.1}$$

with $tr(\cdot)$ the trace. The associated inner product is $\langle A \ , \ B \rangle_F = tr(A^T \cdot B)$. The Frobenius norm is compatible with the 2-norm so that $\|Ax\|_2 \leq \|A\|_F \cdot \|x\|_2$, with $A \in R^{m \times n}$ and $x \in R^n$.

2.2 Feedforward MLP

MLP is a network of simple neurons called perceptrons. The perceptron computes a single output from multiple real-valued inputs by forming a linear combination according to its input weights and then possibly putting the output through some nonlinear activation function. The output is defined as

$$y_k = \sigma(\sum_{i=1}^{n} \omega_{ki} \cdot x_i) \tag{2.2}$$

where the $\sigma(\cdot)$ is activation function of the neuron, n is the number of inputs to the neuron k, ω_{ki} is the weight matrix. In general, we choose $\sigma(\cdot)$ as the following three types:

1. Threshhold function an example of which is

$$\sigma(x) = \begin{cases} 1 & if \ x \geq 0 \\ 0 & if \ x < 0 \end{cases}$$

   This function is also termed the Heaviside function.

2. Piecewise Linear

$$\sigma(x) = \begin{cases} 1 & if \ x \geq ½ \\ x & if \ ½ > x > -½ \\ 0 & if \ x \leq -½ \end{cases}$$

3. Sigmoid Examples include

- Logistic function whose domain is $[0, 1]$

$$\sigma(x) = \frac{1}{1+e^{-\alpha x}}$$

- The hyperbolic tangent whose domain is [-1, -1]

$$\sigma(x) = \frac{1-e^{-\alpha x}}{1+e^{-\alpha s}}$$

- Algebraic sigmoid function whose domain is [-1, -1]

$$\sigma(x) = \frac{x}{\sqrt{1+x^2}}$$

It has been proved that any sufficiently smooth function can be approximated arbitrarily closely on a compact set using a two-layer NN with appropriate weight [50, 51, 52]. For the purpose of adaptive control design, this property of neural network is always used to approximate continuous unknown nonlinear functions.

In this thesis, we will adopt a three-layer feed-forward neural network to work as a part of our controller for the robot manipulator. Figure 2-1 shows the structure of a three-layer neural network.

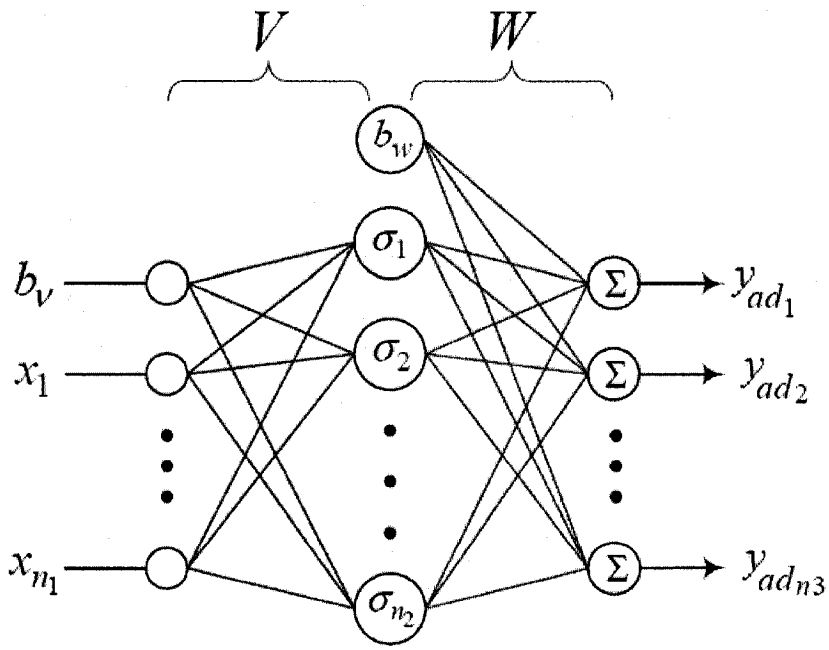

Figure 2-1 Three-layer neural network structure

In Figure 2-1, we denote that $x=[x_1 \quad x_2 \quad ... \quad x_{n1}]^T$ the input layer; $\sigma(\cdot)=[\sigma(\cdot)_1 \quad \sigma(\cdot)_2 \quad ... \quad \sigma(\cdot)_{n2}]^T$ the hidden-layer; and $y=[y_1 \quad y_2 \quad ... \quad y_{n3}{}^2]^T$ the output layer. If we define the three-layer weight matrix and bias vector as $V^T=v_{n2n1}$, b_v and $W^T=w_{n3n2}$, b_w respectively, the output of MLP is obtained as

$$y_j=\sum_{k=1}^{n2}\left[w_{jk}\cdot\sigma\left[\sum_{i=1}^{n1}v_{n2i}\cdot x_i+b_v\right]+b_w\right] \qquad j=1,2,...n3 \tag{2.3}$$

Or in matrix form

$$y=W^T\cdot\sigma(V^T\cdot x+\theta_v)+\theta_w \tag{2.4}$$

Here the activation function between input-layer and hidden-layer is set as purelin and the activation function between hidden-layer and output-layer is defined as $\sigma(\cdot)$.

We can add the bias b_v into the weight matrix $V^T = v_{n2n1}$ as the first column and set the input vector as $x = [x_0 \quad x_1 \quad \ldots \quad x_{n1+1}]^T$ with $x_0 \equiv 1$. Handling the b_w and $W^T = w_{n3n2}$ in the same way, we have

$$y = W^T \cdot \sigma(V^T \cdot x) \tag{2.5}$$

Let S be a compact set of R^n, define $C^n(S)$ be the space such that the map $f(x) : S \to R^n$ is continuous. The NN (Eq. 2.5) can approximate function $f(x) \in C^n(S), \ x \in R^n$ as

$$f(x) = W^T \cdot \sigma(V^T \cdot x) + \varepsilon(x) \tag{2.6}$$

where $\varepsilon(x)$ a functional restructure error vector. If the nominal value of weight matrix W^T does exist to prove $\varepsilon(x) = 0$, we claim that $f(x)$ is in the range of neural network.

Remark 2.1: The nominal weight matrix is bounded by known constant

$$\|W\| \le W_N \tag{2.7}$$

Remark 2.2: Assume restructure error vector $\varepsilon(x)$ is bounded by known constant

$$\|\varepsilon(x)\| \le \varepsilon_N \tag{2.8}$$

2.3 Augmented Feedforward MLP

2.3.1 Mechanism and Structure

Although MLP is proved to approximate the sufficiently smooth function to any accuracy, it needs large number of NN nodes and training iterations to approximate non-smooth functions (i.e. piecewise continuous), which are very common in most real

industrial control systems. Such examples are friction, hysteresis, backlash and other motion control actuator nonlinearities. For these piecewise continuous functions, the feedforward MLP needs to be augmented to work as a function approximator. Results for approximation of piecewise continuous functions or functions with jumps are given in [53, 54].

Let S be a compact set of R^n, define $C^n(S)$ be the space such that the map $f(x): S \to R^n$ is continuous. The NN Eq. (2.6) can approximate a function $f(x) \in C^n(S)$, $x \in R^n$, which has a jump at $x = c$ and is continuous from the right as

$$f(x) = W^T \cdot \sigma(V^T \cdot x) + W_f{}^T \cdot \varphi[V_f{}^T \cdot (x - c)] + \varepsilon(x) \tag{2.9}$$

where $\sigma(\cdot)$, $\varphi(\cdot)$ are the activation functions with $\sigma(\cdot)$ a sigmoid basis function and $\varphi(\cdot)$ has the definition $\varphi(\cdot) = \begin{cases} 0 & x < c \\ \left(\dfrac{1 - e^{-\alpha \cdot x}}{1 + e^{-\alpha \cdot x}}\right)^k & x \geq c \end{cases}$, $\varepsilon(x)$ is a functional restructure error vector and W^T, $W_f{}^T$ and V^T, V^T is an ideal constant weight matrix. The structure of the augmented feedforward MLP is shown in Figure 2-2

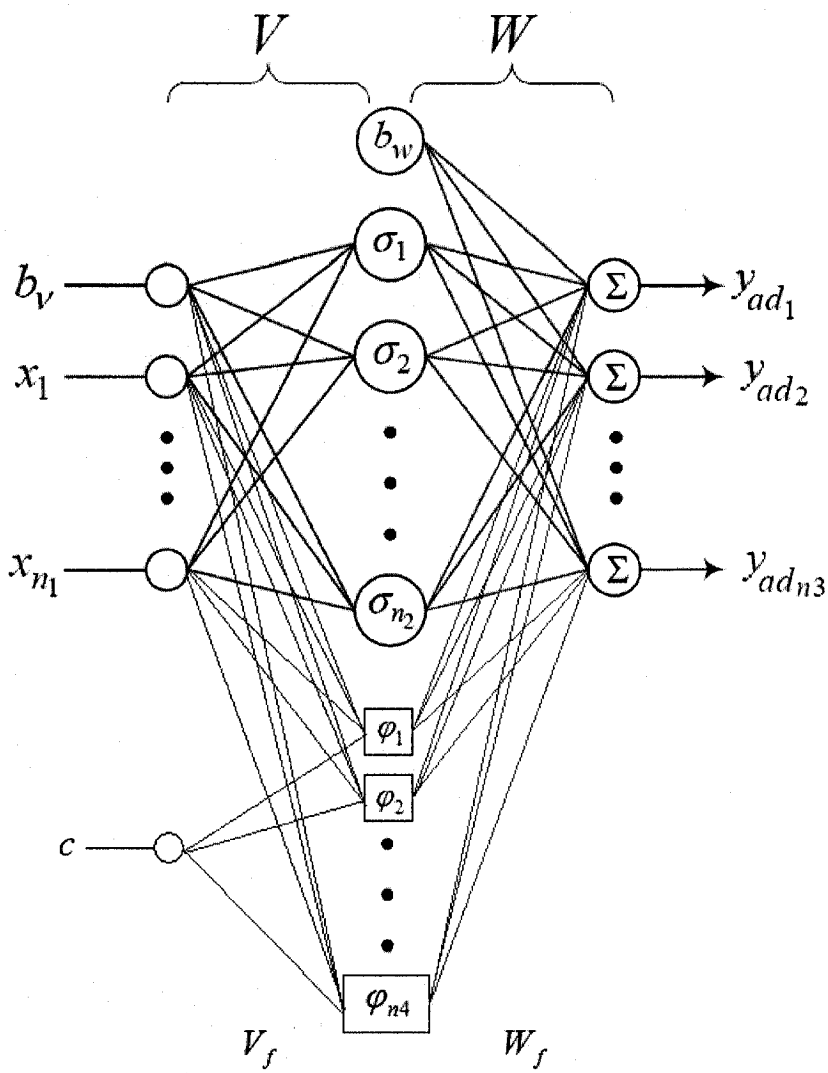

Figure 2-2 Augmented MLP structure

In this thesis, it is assumed that there exists such a weight matrix that $\|\varepsilon(x)\| \le \varepsilon_N$ with constant $\varepsilon_N > 0$, for all $x \in R^n$, and the norm of the matrix is bounded by a known constant $\|W\| \le W_N$ with $W_N > 0$.

2.3.2 Piecewise continuous function-examples

Friction is a nonlinear phenomenon, which exist in almost all robot manipulator. It depends on the system's internal state such as contacting surface, lubricant, and temperature. It can affect the overall performance of robot manipulator, including both static and dynamic stability. It introduces tracking error and causes even system instability.

The friction is usually modeled as a piecewise continuous function of velocity and friction torque, which depends on the sign of velocity.

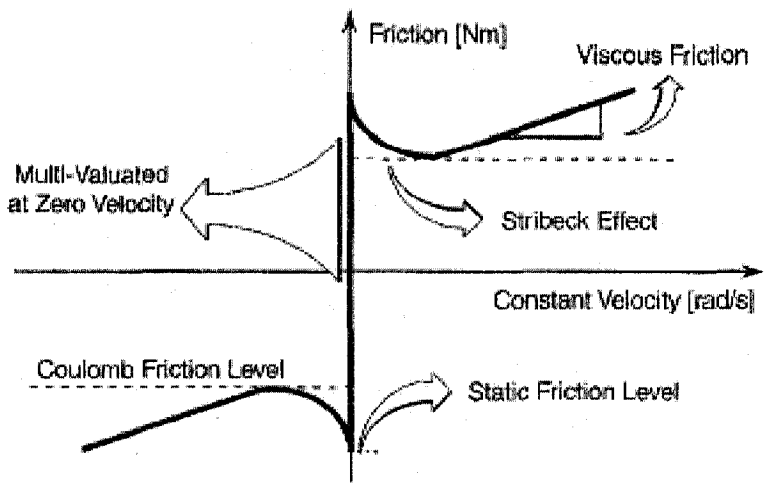

Figure 2-3 Fiction description [55]

The friction models such as Coulomb friction and viscous friction are introduced in [56] as.

$$F(\dot{q}) = \sigma_0 \cdot z + \sigma_1 \frac{dz}{dt} + \sigma_2 \cdot v \tag{2.10}$$

where σ_0 is the stiffness, σ_1 is a damping coefficient and σ_2 is a term account for

viscous friction; v is relative velocity between the two surface. z is a internal state of the system and it has the form as

$$z = g(v) \cdot \text{sgn}(v) \tag{2.11}$$

The friction model given Eq. (2.10) and Eq. (2.11) is characterized by function $g(v)$ and parameters σ_0, σ_1, and σ_2. A detailed friction model for industrial controller design is also given in [56] as:

$$F(\dot{q}) = [\alpha_0 + \alpha_1 \cdot e^{-\beta_1|\dot{q}|} + \alpha_2(1 - e^{-\beta_2|\dot{q}|})] \cdot \text{sgn}(\dot{q}) \tag{2.12}$$

where α_0, α_1 represent static friction; α_2 represents the viscous friction.

Friction model in Eq. (2.12) is highly nonlinear and discontinuous at zero. It can be approximated by the augmented feedforward MLP in Eq. (2.9). Moreover, it is found that the presented augment feedforward MLP has the ability to approximate functions with jumps suitably [53,54].

2.5 Conclusion

In this chapter, the structure and the main definitions of the MLP are introduced. An important mathematical preliminary is given for the further utility. The basic mechanism and structure of feedforward MLP used in function approximation are given. An augmented feedforward MLP structure for piecewise continuous function approximation is also introduce with an example.

Chapter 3 NN based Adaptive Controller Design for RLFJ Robot Manipulator

A large number of control strategies have been proposed for the control of robot manipulators because of their widely usage in today's industry. When taking joints' elasticity into account, integral manifold can reduce the order of the flexible robot manipulator dynamics by decomposing the system model into fast subsystem and slow subsystem. As a useful tool for designing the control schemes for RLFJ robot manipulators, its seeming drawbacks are complexity in deriving the expression of the slow control and the computational cost of implementation. In this chapter, a composite approach to adaptive NN controller is proposed for the RLFJ robot manipulator with unknown nonlinearities. Those computation burdens are avoidable by using the NN as the function approximator

3.1 Robot Dynamic model

An accurate dynamic model is very important for designing the model-based control scheme. There are several approaches have been used in deriving the dynamic model of a nonlinear system such as Lagrangian formulation and Newton-Euler equation. This Section provides the background required for the robot manipulator, which is derived in the Lagrange-Euler equation formulation. Some important properties of the robot dynamic model are introduced.

3.1.1 Lagrange's Equation and Model Expansion

Lagrange's Equation is a most frequently used method for a conservative system [57]

$$\frac{d}{dt}\frac{\partial L}{\partial \dot{q}} - \frac{\partial L}{\partial q} = \tau \tag{3.1}$$

where q the joint variables is generalized coordinates, τ is torque and force on the joint, and the lagrangian is the different between the kinetic energy K_L and potential energy P

$$L = K_L - P \tag{3.2}$$

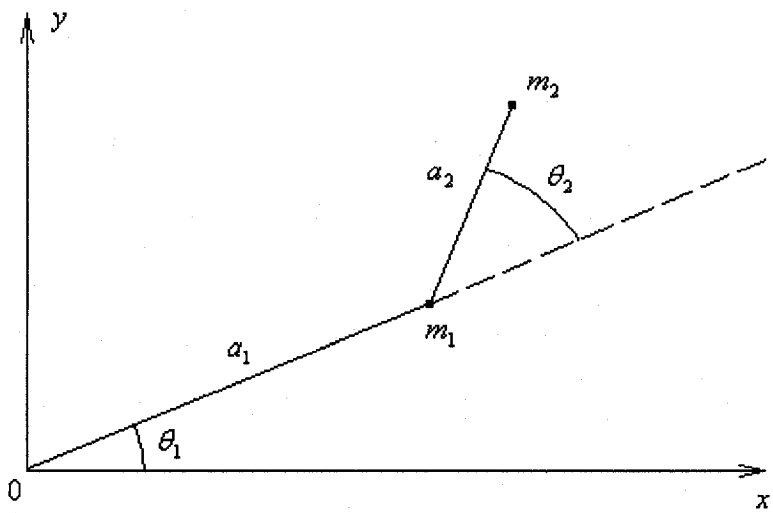

Figure 3-1 Two-link RR manipulator

In Figure 3-1, the robot manipulator is a two-link RR arm. To make the question easier, we assume that the link mass are concentrated at the end of the links. We can write the robot manipulator dynamic equation in vector and matrix form as

$$\begin{bmatrix} (m_1+m_2)a_1^{\,2}+m_2\cdot a_2^{\,2}+2m_2a_1a_2\cdot\cos\theta_2 & m_2\cdot a_2^{\,2}+m_2a_1a_2\cdot\cos\theta_2 \\ m_2\cdot a_2^{\,2}+m_2a_1a_2\cdot\cos\theta_2 & m_2\cdot a_2^{\,2} \end{bmatrix}\begin{bmatrix} \ddot{\theta}_1 \\ \ddot{\theta}_2 \end{bmatrix}$$
$$+\begin{bmatrix} -m_2a_1a_2(2\dot{\theta}_1\dot{\theta}_2+\dot{\theta}_2^{\,2})\sin\theta_2 \\ m_2a_1a_2\cdot\dot{\theta}_1^{\,2}\cdot\sin\theta_2 \end{bmatrix}+\begin{bmatrix} (m_1+m_2)g\cdot a_1\cdot\cos\theta_1+m_2g\cdot a_2\cdot\cos(\theta_1+\theta_2) \\ m_2g\cdot a_2\cdot\cos(\theta_1+\theta_2) \end{bmatrix}$$
$$=\begin{bmatrix} \tau_1 \\ \tau_2 \end{bmatrix} \tag{3.3}$$

Define

$$M(q)=\begin{bmatrix} (m_1+m_2)a_1^{\,2}+m_2\cdot a_2^{\,2}+2m_2a_1a_2\cdot\cos\theta_2 & m_2\cdot a_2^{\,2}+m_2a_1a_2\cdot\cos\theta_2 \\ m_2\cdot a_2^{\,2}+m_2a_1a_2\cdot\cos\theta_2 & m_2\cdot a_2^{\,2} \end{bmatrix} \tag{3.4}$$

$$V(q,\dot{q})=\begin{bmatrix} -m_2a_1a_2(2\dot{\theta}_1\dot{\theta}_2+\dot{\theta}_2^{\,2})\sin\theta_2 \\ m_2a_1a_2\cdot\dot{\theta}_1^{\,2}\cdot\sin\theta_2 \end{bmatrix} \tag{3.5}$$

$$G(q)=\begin{bmatrix} (m_1+m_2)g\cdot a_1\cdot\cos\theta_1+m_2g\cdot a_2\cdot\cos(\theta_1+\theta_2) \\ m_2g\cdot a_2\cdot\cos(\theta_1+\theta_2) \end{bmatrix} \tag{3.6}$$

and considering friction and disturbances, Eq. (3.3) can be rewritten as

$$M(q)\cdot\ddot{q}+V(q,\dot{q})+G(q)+F(\dot{q})+T_L=\tau \tag{3.7}$$

where $M(q)\in R^{n\times n}$ the inertia matrix, $V(q,\dot{q})\in R^{n\times n}$ the coriolis and centripetal vector, $G(q)\in R^n$ the gravity vector, $F(\dot{q})$ the friction, and T_L the disturbance.

3.1.2 Properties of the Robot Dynamics

Properties 3.1: boundedness of the inertia matrix

From the definition of inertia Matrix $M(q)$ in Eq. (3.7), it's obvious that $M(q)$ is a symmetric, positive-definite and a nonlinear function of q and it's bounded by

$$m_1\cdot I\le M(q)\le m_2\cdot I \tag{3.8}$$

where m_1, m_2 are known positive constants

Properties 3.2: skew symmetry

The coriolis and centripetal vector $V(q,\dot{q})$ can be written as

$$V(q,\dot{q}) = V_m(q,\dot{q}) \cdot \dot{q} \tag{3.9}$$

The matrix $\dot{M} - 2V_m$ is skew-symmetric.

$$\dot{q}^T \cdot (\dot{M} - 2V_m) \cdot \dot{q} = 0 \tag{3.10}$$

Properties 3.3: gravity, friction and disturbance boundedness

From the robot manipulator dynamic model, the bounds on the gravity term, friction term, and disturbance can be derived

$$\|G(q)\| \le g_b(q) \tag{3.11}$$

$$\|F(\dot{q})\| \le f_b \cdot \|\dot{q}\| + d_b \tag{3.12}$$

$$\|T_L\| \le a_b \tag{3.13}$$

where $g_b(q)$, f_b, d_b, a_b are positive scalars.

3.1.3 Dynamics with Joint Flexibility

In reality, the robot manipulator joint motor coupled to a load through a shaft that usually has significant flexibility as shown in Figure 3-2.

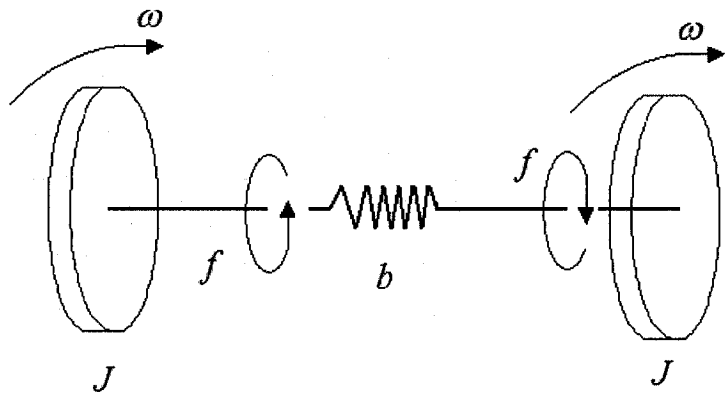

Figure 3-2 Motor with shaft compliance

If the motor inertia defined as a diagonal matrix $J = J^T \in R^{n\times n}$, the joint damping term as a diagonal matrix $B = B^T \in R^{n\times n}$, and the stiffness coefficients matrix as a diagonal matrix $K = K^T \in R^{n\times n}$, the flexible joints robot manipulator system dynamic model becomes

$$M(q)\cdot\ddot{q} + V_m(q,\dot{q})\cdot\dot{q} + G(q) + F(\dot{q}) + T_L + K\cdot(q - q_f) = 0 \tag{3.14a}$$

$$J\cdot\ddot{q}_f + B\cdot\dot{q}_f - K\cdot(q - q_f) = \tau \tag{3.14b}$$

where $q,\dot{q},\ddot{q} \in R^n$ refer to the link position, velocity and acceleration, respectively, $q_f,\dot{q}_f,\ddot{q}_f \in R^n$, the motor shaft angle, angular velocity and angular acceleration, individually, $T_L \in R^n$ the load disturbance, and τ the control torque.

When taking the joints flexibility into account, we need to double the state variables in the dynamic model. This causes that the dynamic model of a flexible joint robot is of order four instead of order two for a rigid robot. Thus, the control problem becomes more complicated when the joint flexibility is considered.

Since joint stiffness is large compared with other parameters, we assume

$$K = K_1/\gamma^2 \tag{3.15}$$

where γ is a small parameter representing the inverse of stiffness and K_1 is on the order of 1. Suppose J and B are very small and on the same order of γ. The rigid model can be derived from Eq. (3.14a) and Eq. (3.14b) by assuming no elasticity at the joints (i.e. $\gamma = 0$) and is given by:

$$[M(q) + J] \cdot \ddot{q} + [V_m(q,\dot{q}) + B] \cdot \dot{q} + G(q) + F(\dot{q}) + T_L = \tau \tag{3.16}$$

Since the J and B are very small comparing with $M(q)$ and $V(q,\dot{q})$, Eq. (3.16) becomes Eq. (3.7).

3.2 Control Objective

The control objective is to develop a position-tracking controller for an unknown RLFJ robot dynamics Eq. (3.14a) and Eq. (3.14b) so that the link position follows a desired trajectory. The tracking error of the robot is defined as

$$e(t) = q_d(t) - q(t) \tag{3.17}$$

where $q_d(t) \in R^n$ is the given desired trajectory, which is continuous, and its derivatives up to higher order are bounded.

A filtered error is defined as

$$r = \dot{e} + \Lambda \cdot e \tag{3.18}$$

where $\Lambda = \Lambda^T > 0$

The elasticity at the joints is large enough so that the system can be decomposed into

a "slow" subsystem and a "fast" subsystem. From [22], the control signal τ for the whole system has the form as

$$\tau = \tau_s + \tau_f \tag{3.19}$$

where τ_s is the slow part and τ_f is the fast part, which is defined as:

$$\tau_f = K_f(\dot{q} - \dot{q}_f) \tag{3.20}$$

Usually, we choose

$$K_f = K_2/\gamma \tag{3.21}$$

with K_2 on the order of 1.

Define z as the difference between the link and motor position

$$z = q_f - q \tag{3.22}$$

The RLFJ robot manipulator dynamics becomes

$$M(q)\cdot\ddot{q} + V_m(q,\dot{q})\cdot\dot{q} + G(q) + F(\dot{q}) + T_L - K\cdot z = 0 \tag{3.23}$$

$$J\cdot\ddot{q}_f + B\cdot\dot{q}_f + K\cdot z = \tau \tag{3.24}$$

Substituting control signal τ Eq. (3.19), Eq. (3.20) and Eq. (3.22) into system Eq. (3.24), one obtains:

$$J\cdot\ddot{z} + (B + K_f)\cdot\dot{z} + K\cdot z = \tau_s - J\cdot\ddot{q} - B\cdot\dot{q} \tag{3.25}$$

Define an integral manifold as $h = K\cdot z$ and rewrite Eq. (3.25) as

$$J\cdot\ddot{h} + (B + K_f)\cdot\dot{h} + K\cdot h = K(\tau_s - J\cdot\ddot{q} - B\cdot\dot{q}) \tag{3.26}$$

where $h = h(t,\gamma,q,q_f)$.

Under the assumptions Eq. (3.15) and Eq. (3.21), one obtains

$$\gamma^2\cdot J\cdot\ddot{h} + \gamma\cdot(\gamma\cdot B + K_2)\cdot\dot{h} + K_1\cdot h = K_1(\tau_s - J\cdot\ddot{q} - B\cdot\dot{q}) \tag{3.27}$$

An approximate reduced-order flexible model can be derived by using a power series expansion of the integral manifold h and control τ_s around $\gamma = 0$. It is found that the slow control component τ_s is independent of fast control component τ_f. Let us denote:

$$\begin{aligned} h &= h_0 + \gamma h_1 + O(\gamma^2) \\ \tau_s &= \tau_0 + \gamma \tau_1 + O(\gamma^2) \end{aligned} \tag{3.28}$$

where τ_0 is the control input to the rigid model, τ_1 is the corrective torque term for compensating the effects of γ, the vector h_0 represents a zeroth-order approximation of h and the h_1 represents the first order correction to h_0.

By substituting Eq. (3.28) into Eq. (3.26), we get

$$\gamma^2 J \cdot \ddot{h}_1 + O(\gamma^3) + \gamma(\gamma \cdot B + K_2)\dot{h}_0 + \gamma^2(\gamma B + K_f)\dot{h}_1 + O(\gamma^3) + K_1 \cdot h_0 + \gamma K_1 h_1 + O(\gamma^2)$$

$$= K_1 \cdot \tau_0 + \gamma K_1 \cdot \tau_1 + O(\gamma^2) - K_1 J \cdot \ddot{q} - K_1 B \cdot \dot{q} \tag{3.29}$$

By equating terms of the same powers of γ on both sides of Eq. (3.29), we get

γ^1 terms: $K_2 \cdot \dot{h}_0 + K_1 h_1 = K_1 \cdot \tau_1$ (3.30)

γ^0 terms: $K_1 h_0 = K_1 \cdot \tau_0 - KJ \cdot \ddot{q} - KB \cdot \dot{q}$ (3.31)

From Eq. (3.30), we obtain:

$$h_1 = K_1^{-1}(K_1 \cdot \tau_1 - K_2 \cdot \dot{h}_0) \tag{3.32}$$

and Eq. (3.31) is written as :

$$h_0 = K_1^{-1}(K_1 \cdot \tau_0 - KJ \cdot \ddot{q} - KB \cdot \dot{q}) \tag{3.33}$$

Eq. (3.32) tells us that the corrective control τ_1 relates to h_1 and rigid control τ_0 relates to h_0.

From Eq. (3.27), the integral manifold h becomes:

$$h = (\tau_s - J \cdot \ddot{q} - B \cdot \dot{q}) - K_1^{-1}[\gamma \cdot J \cdot \dddot{h} + \gamma \cdot (\gamma \cdot B + K_2) \cdot \ddot{h}] \tag{3.34}$$

After substitution for $K \cdot z$ in Eq. (3. 23) and usage of Eq. (3.28), the system Eq. (3.23) is rewritten as

$$M(q) \cdot \ddot{q} + V_m(q, \dot{q}) \cdot \dot{q} + G(q) + F(\dot{q}) + T_L$$

$$= \tau_s - J \cdot \ddot{q} - B \cdot \dot{q} - \gamma \cdot K_1^{-1}[\gamma \cdot J \cdot \ddot{h}_0 + (\gamma \cdot B + K_2) \cdot \dot{h}_0] + O(\gamma^2) \tag{3.35}$$

The variables $\ddot{h}_0$ and $\dot{h}_0$ are "fast" variables; the link variables q and $\dot{q}$ are "slow" variables. Moreover, the rigid model Eq. (3.16) is obtained by setting $\gamma = 0$.

The control task is to design τ_0 and τ_1 so that the link position of robot follows the desired trajectory. Both τ_0 and τ_1 are derived with complicate expression especially in the adaptive integral manifold method [23]. In control application, NN is usually used as a tool for modeling nonlinear function due to their universal function approximation capability. In order to alleviate the symbolic computational burden in calculating τ_0 and τ_1, two three-layer MLP are utilized to approximate two complicate nonlinear functions to form the control signals τ_0 and τ_1.

3.3 Rigid Joint Case

The control signal τ_0 is designed by considering the rigid joint model Eq. (3.16). Combining the filtered error Eq. (3.18) and system dynamics Eq. (3.14a) and Eq. (3.14a), one may obtain:

$$[M + J] \cdot \dot{r} = F_0 - [V_m + B] \cdot r - \tau_0 + T_L \tag{3.36}$$

where F_0 is a complicated nonlinear function defined as

$$F_0 = M(q) \cdot (\ddot{q}_d + \Lambda \dot{e}) + V_m(q, \dot{q}) \cdot (\dot{q}_d + \Lambda e) + G(q) + F(\dot{q}) \tag{3.37}$$

Motivated by the universal approximate capability of NN, we utilize a first-layer-fixed MLP to approximate the nonlinear function F_0 Eq. (3.37).

$$F_0 = f_0(x) = W_0^T \cdot \sigma(V^T \cdot x) + \varepsilon_0(x) \tag{3.38}$$

$$\hat{F}_0 = \hat{f}_0(x) = \hat{W}_0^T \cdot \sigma(V^T \cdot x) \tag{3.39}$$

where $x = \left[\ddot{q}^T \quad \dot{q}^T \quad q^T \quad \ddot{q}_d^T \quad \dot{q}_d^T \quad \text{sgn}(\dot{q})^T \quad 1\right]^T$, input-layer weight matrix V^T is pre-fixed and $\hat{W}_0^T$ is the estimated output-layer weight matrix W_0^T.

Define the weight estimation error as

$$\tilde{W}_0^T = W_0^T - \hat{W}_0^T \tag{3.40}$$

The RLRJ controller is designed as

$$\tau_0 = \hat{F}_0 + K_v \cdot r \tag{3.41}$$

where r is the filtered error and K_v is a gain matrix.

The update rule of the NN is designed as

$$\dot{\hat{W}} = \Gamma \cdot \sigma(V^T \cdot x) \cdot r^T - k \cdot \Gamma \cdot \|r\| \cdot \hat{W} \tag{3.42}$$

where $\Gamma = \Gamma^T > 0$ and $k > 0$.

The stability of controller is proved in the following theorem.

Theorem 3.1

For a RJRL robot Eq. (3.16), the NN controller Eq. (3.41) and update rule Eq. (3.42) are applied. For a desired trajectory $q_d(t)$, it is assumed that its time derivatives up to third order are continuous and bounded. The controlled system's filtered error $r(t)$ is bounded and the tracking error $e(t)$ converges to a small neighbourhood around zero by

appropriately choosing suitable gain matrix K_v.

Proof

Define the Lyapunov function as

$$L_1 = \frac{1}{2} r^T \cdot [M + J] \cdot r + \frac{1}{2} tr(\tilde{W}^T \cdot \Gamma^{-1} \cdot \tilde{W}) \geq 0 \tag{3.43}$$

where M, J are defined in Eq. (3.14a), Eq. (3.14b), and we have Eq. (3.8), $\Gamma = \Gamma^T > 0$.

Differentiating Eq. (3.43) yields

$$\dot{L}_1 = \frac{1}{2}(\dot{r}^T \cdot [M + J] \cdot r + r^T \cdot [M + J] \cdot \dot{r}) + \frac{1}{2} r^T \cdot \dot{M} \cdot r + \frac{1}{2} tr(\dot{\tilde{W}}^T \cdot \Gamma^{-1} \cdot \tilde{W} + \tilde{W}^T \cdot \Gamma^{-1} \cdot \dot{\tilde{W}})$$

$$= r^T \cdot [M + J] \cdot \dot{r} + \frac{1}{2} r^T \cdot \dot{M} \cdot r + tr(\tilde{W}^T \cdot \Gamma^{-1} \cdot \dot{\tilde{W}}). \tag{3.44}$$

Introducing Eq. (3.36), Eq. (3.41) and Eq. (3.42), one gets:

$$\dot{L}_1 = r^T[-(V_m + B + K_v)r + \tilde{F}_0 + T_L] + \frac{1}{2} r^T \cdot \dot{M} \cdot r + tr[\tilde{W}^T \cdot \Gamma^{-1}(-\Gamma \cdot \sigma(V^T \cdot x) \cdot r^T + k \cdot \Gamma \cdot \|r\| \cdot \hat{W})]$$
$$+ tr[\tilde{W}^T \cdot \Gamma^{-1}(-\Gamma \cdot \sigma(V^T \cdot x) \cdot r^T + k \cdot \Gamma \cdot \|r\| \cdot \hat{W})]$$

$$= -r^T \cdot (K_v + B) \cdot r + r^T \cdot \tilde{W}^T \cdot \sigma(V^T \cdot x) + r^T \cdot (T_L + \varepsilon_0) + \frac{1}{2} r^T \cdot (\dot{M} - 2V_m) \cdot r$$

$$+ tr[-\tilde{W}^T \cdot \sigma(V^T \cdot x) \cdot r^T + \tilde{W}^T \cdot k \cdot \|r\| \cdot \hat{W})]$$

$$= -r^T \cdot (K_v + B) \cdot r + r^T \cdot (T_L + \varepsilon_0) + k \cdot \|r\| \cdot tr[\tilde{W}^T (W - \tilde{W})]$$

$$= -r^T \cdot (K_v + B) \cdot r + r^T \cdot (T_L + \varepsilon_0) + k \cdot \|r\| \cdot tr(\tilde{W}^T \cdot W - \|\tilde{W}^T\|^2) \tag{3.45}$$

Since B is very small compared with K_v, its influence can be omitted. The minimum eigenvalue of gain matrix K_v is $\lambda_{v\min}$. Thus we have

$$\dot{L}_1 \le -\lambda_{v\min}\cdot\|r\|^2 + \|r\|\cdot(a_d+\varepsilon_N) + k\cdot\|r\|\cdot tr(\tilde{W}^T\cdot W - \|\tilde{W}^T\|^2)$$

$$\le -\lambda_{v\min}\cdot\|r\|^2 + \|r\|\cdot(a_d+\varepsilon_N) + k\cdot\|r\|\cdot\|\tilde{W}\|(W_N - \|\tilde{W}\|)$$

$$\le -\lambda_{v\min}\cdot\|r\|^2 + \|r\|[(a_d+\varepsilon_N) + k\cdot\|\tilde{W}\|\cdot W_N - k\cdot\|\tilde{W}\|^2]$$

$$= -\|r\|\left[\lambda_{v\min}\cdot\|r\| - (a_d+\varepsilon_N) + k\cdot(\|\tilde{W}\| - \frac{W_N}{2})^2 - k\cdot\frac{W_N^2}{4}\right]$$

$$\le -\|r\|\left[\lambda_{v\min}\cdot\|r\| - (a_d+\varepsilon_N) - k\cdot\frac{W_N^2}{4}\right]$$

where $a_d+\varepsilon_N$ is the upper bound of $T_L+\varepsilon_0$.

If we have

$$\|r\| > \frac{k\cdot W_N{}^2/4 + (a_d+\varepsilon_N)}{\lambda_{v\min}} \tag{3.46}$$

Or

$$\|\tilde{W}\| > W_N/2 + \sqrt{W_N{}^2/4 + (a_d+\varepsilon_N)/k} \tag{3.47}$$

, we can prove that $\dot{L}_1$ negative. Inequality (3.52) shows that if the control gain K_v is chosen large enough so that

$$\frac{k\cdot W_N{}^2/4 + (a_d+\varepsilon_N)}{\lambda_{v\min}} < b_r \tag{3.48}$$

where $b_r > 0$ represents the radius of a ball inside the compact set C_r of filtered error $r(t)$.

Thus, any trajectory $r(t)$ starting in compact set $C_r = \{r \mid \|r\| \le b_r\}$ converges within C_r and is bounded. Then tracking error $e(t)$ converges to a small neighbourhood around zero. According to the standard Lyapunov theorem extension [45],

this demonstrates the UUB (uniformly ultimately bounded) of both $r(t)$ and $\tilde{W}$.

3.4 Flexible Joint Case

Introducing tracking error Eq. (3.39) into system Eq. (3.35), we get

$$M \cdot \dot{r} = -V_m \cdot r + F_0 - \tau_s + T_L + J \cdot \ddot{q} + B \cdot \dot{q} + \gamma \cdot K_1^{-1}[\gamma \cdot J \cdot \ddot{h}_0 + (\gamma \cdot B + K_2) \cdot \dot{h}_0] \qquad (3.49)$$

From Eq. (3.28), we obtain:

$$M \cdot \dot{r} = -V_m \cdot r + F_0 - \tau_0 - \gamma \cdot \tau_1 - O(\gamma^2) + T_L +$$

$$\gamma \cdot \left\{K_1^{-1}[\gamma \cdot J \cdot \ddot{h}_0 + (\gamma \cdot B + K_2) \cdot \dot{h}_0] + K_2^{-1} \cdot K_f[J \cdot \ddot{q} + B \cdot \dot{q}]\right\} \qquad (3.50)$$

If the nonlinear function F_1 is defined as

$$F_1 = K_1^{-1}[\gamma \cdot J \cdot \ddot{h}_0 + (\gamma \cdot B + K_2) \cdot \dot{h}_0] + K_2^{-1} \cdot K_f[J \cdot \ddot{q} + B \cdot \dot{q}] \qquad (3.51)$$

, we derive the error dynamics as:

$$M \cdot \dot{r} = -V_m \cdot r + F_0 - \tau_0 - \gamma \cdot \tau_1 - O(\gamma^2) + \gamma \cdot F_1 + T_L. \qquad (3.52)$$

To implement F_1 Eq. (3.51), we need to compute $\dot{h}_0$ and $\ddot{h}_0$. They can be obtained by differentiating Eq. (3.33) and using $\ddot{q}$ from the rigid model Eq. (3.16). Since h_0 is a nonlinear function related to rigid control τ_0, F_1 is highly complex nonlinear function of τ_0, q, $\dot{q}$, and $\ddot{q}$.

Again, we utilize a second first-layer-fixed MLP to approximate the nonlinear function F_1 Eq. (3.52).

$$F_1 = f_1(y) = W_1^T \cdot \sigma(V^T \cdot y) + \varepsilon_1(y) \qquad (3.53)$$

where $y = \begin{bmatrix} \tau_0^T & q^T & \dot{q}^T & \ddot{q}^T & 1 \end{bmatrix}^T$.

The corrective term is designed as:

$$\tau_1 = \hat{F}_1 + K_u \cdot \varphi \tag{3.54}$$

where φ is a fictitious variable, which will be designed later.

Substituting the control strategy Eq. (3.41) and Eq. (3.54) into the error dynamics Eq. (3.52), one obtains:

$$M \cdot \dot{r} = -V_m \cdot r + F_0 - \tau_0 - \gamma \cdot \tau_1 - O(\gamma^2) + \gamma \cdot F_1 + T_L$$

$$M \cdot \dot{r} = -(V_m + K_v) \cdot r - \gamma \cdot K_u \cdot \varphi + \tilde{F}_0 + \gamma \cdot \tilde{F}_1 + T_L \tag{3.55}$$

Design fictitious variable as

$$\dot{\varphi} = \tau_0 - K \cdot z \tag{3.56}$$

Using Eq. (3.28) and Eq. (3.24), one has

$$\dot{\varphi} = \tau_0 - (\tau_s - J \cdot \ddot{q} - B \cdot \dot{q}) + [K_1^{-1}\gamma^2 \cdot J \cdot \dddot{h} + K_1^{-1}\gamma \cdot (\gamma \cdot B + K_2) \cdot \ddot{h}]$$

$$\dot{\varphi} = -\gamma \cdot \tau_1 - O(\gamma^2) + \gamma \cdot [K_1^{-1}\gamma \cdot J \cdot \dddot{h} + K_1^{-1}(\gamma \cdot B + K_2) \cdot \ddot{h} + K_f \cdot K_2^{-1}(J \cdot \dddot{q} + B\ddot{q})] \tag{3.57}$$

Using Eq. (3.51), we get

$$\dot{\varphi} = \gamma \cdot F_1 - \gamma \cdot \tau_1 - O(\gamma^2) \tag{3.58}$$

Similarly, with the control strategy Eq. (3.54), and Eq. (3.58) becomes

$$\dot{\varphi} = \gamma \cdot \tilde{F}_1 - \gamma \cdot K_u \cdot \varphi \tag{3.59}$$

Now, we have two different NNs based controllers—one is the first slow part τ_0 based on a rigid NN F_0 function and the other is the second slow part τ_1 based on the corrective NN F_1 function. The composite control scheme is shown as:

$$\tau = \tau_s + \tau_f = \tau_0 + \gamma \cdot \tau_1 + O(\gamma^2) - K_f \dot{z} \tag{3.60}$$

With Eq. (3.41) and Eq. (3.44), the overall control scheme is derived as shown in

Figure 3-3

$$\tau = (\hat{F}_0 + K_v \cdot r) + \gamma \cdot (\hat{F}_1 + K_u \cdot \varphi) - K_f \dot{z} \quad . \tag{3.61}$$

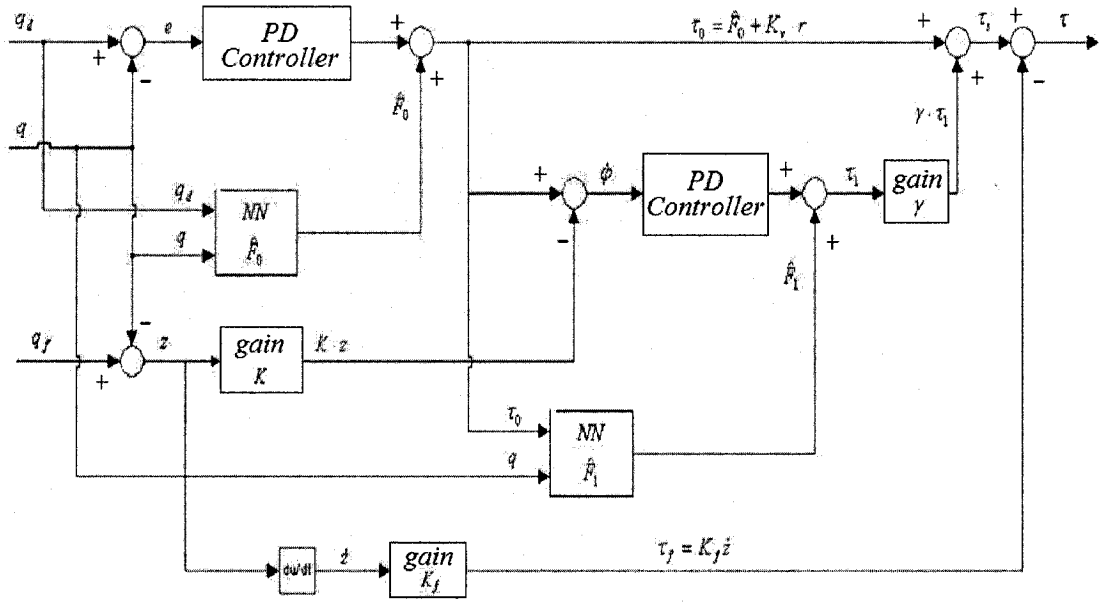

Figure 3-3 NN Controller structure

Choose the update rule for those weight matrix respectively as

$$\dot{\hat{W}}_0 = \Gamma_0 \cdot \sigma_0(V^T \cdot x) \cdot r^T - k \cdot \Gamma_0 \cdot \|\xi\| \cdot \hat{W}_0 \tag{3.62}$$

$$\dot{\hat{W}}_1 = \Gamma_1 \cdot \sigma_1(V^T \cdot y) \cdot (\varphi^T + r^T) - k \cdot \Gamma_1 \cdot \|\xi\| \cdot \hat{W}_1 \tag{3.63}$$

where $\xi = \begin{bmatrix} r^T & \varphi^T \end{bmatrix}^T, \Gamma = \Gamma^T > 0$ and $k > 0$,

and the weight matrix errors are derived as:

$$\dot{\tilde{W}}_0 = -\dot{\hat{W}}_0 = -\Gamma_0 \cdot \sigma_0(V^T \cdot x) \cdot r^T + k \cdot \Gamma_0 \cdot \|\xi\| \cdot \hat{W}_0 \tag{3.64}$$

$$\dot{\tilde{W}}_1 = -\dot{\hat{W}}_1 = -\Gamma_1 \cdot \sigma_1(V^T \cdot y) \cdot (\varphi^T + r^T) + k \cdot \Gamma_1 \cdot \|\xi\| \cdot \hat{W}_1 \tag{3.65}$$

For comparison, to design a controller by traditional singular perturbation strategy, the procedure is much more complicated, tedious and time-consuming [24]. Firstly, the system dynamics must be rewritten in form of designed integral manifold and new system internal variables. Secondly, the recovery of the rigid model needs to be satisfied by calculating the initial values of a series of new system coefficients. Thirdly, by using Taylor series expansion around the zero of the integral manifold, the reduced-order flexible model is obtained. Still, a series of new timers need to be computed recursively by the form of differential equations. Finally, the controller for rigid case and corrective term for joint flexibility is designed.

Another control strategy is also proposed to combine NN with traditional control scheme for flexible joint robot [13]. Three fictitious error terms and control signal is designed. Then, three NNs are used in those three new error dynamics. Not only the controller structure but also the weight matrix update rules are more complex than our controller.

Remark 3.1: The NN controller design algorithm was motivated by the integral manifold method. In integral manifold procedure, an iterative algorithm has been proposed to solve the manifold to which the slow dynamics converges by using Taylor series expansion around the zero of the inverse of stiffness. The procedure becomes very tedious and time-consuming. For different robots with different nonlinear models, the procedure has to be repeated. While the proposed NN controller does not need such computations and are applicable to different robots with different parameters due to the on-line tuning.

Remark 3.2: No off-line weight tuning is needed. The initial estimation values of the

weight matrix $\hat{W}_0^T$ and $\hat{W}_1^T$ are set to zero. At the beginning, the controller becomes a PD controller. The control scheme does not guarantee that $\hat{W}_0^T$ and $\hat{W}_1^T$ converge to the true values of W_0^T and W_1^T. From the above theorem, we may claim that the boundedness of W_0^T, W_1^T and $r(t)$ are guaranteed. Thus, the tracking error $e(t)$ is guaranteed to approach to zero.

Theorem 3.2

For a RJFL robot Eq. (3.14a), Eq. (3.14b), the NN controller Eq. (3.61) and update rule Eq. (3.64), Eq. (3.65) are applied. For a desired trajectory $q_d(t)$, it is assumed that its time derivatives up to third order are continuous and bounded. The controlled system's filtered error $r(t)$ and fictitious variable $\varphi(t)$ are bounded and the tracking error $e(t)$ will converge to a small neighbourhood around zero by appropriately choosing suitable gain matrix K_f, K_v, and K_u.

Proof

Define the Lyapunov function as

$$L_2 = \frac{1}{2} r^T \cdot M \cdot r + \frac{\gamma}{2} \varphi^T \cdot \varphi + \frac{1}{2} tr(\tilde{W}_0^T \cdot \Gamma_0^{-1} \cdot \tilde{W}_0) + \frac{\gamma}{2} tr(\tilde{W}_1^T \cdot \Gamma_1^{-1} \cdot \tilde{W}_1) \geq 0 \qquad (3.66)$$

Differentiating the above function yields

$$\dot{L}_2 = \frac{1}{2}(\dot{r}^T \cdot M \cdot r + r^T \cdot M \cdot \dot{r}) + \frac{1}{2} r^T \cdot \dot{M} \cdot r + \frac{\gamma}{2}(\dot{\varphi}^T \cdot \varphi + \varphi^T \cdot \dot{\varphi})$$

$$+ \frac{1}{2} tr(\dot{\tilde{W}}_0^T \cdot \Gamma_0^{-1} \cdot \tilde{W}_0 + \tilde{W}_0^T \cdot \Gamma_0^{-1} \cdot \dot{\tilde{W}}_0) + \frac{\gamma}{2} tr(\dot{\tilde{W}}_1^T \cdot \Gamma_1^{-1} \cdot \tilde{W}_1 + \tilde{W}_1^T \cdot \Gamma_1^{-1} \cdot \dot{\tilde{W}}_1)$$

$$\dot{L}_2 = r^T \cdot M \cdot \dot{r} + \frac{1}{2} r^T \cdot \dot{M} \cdot r + \gamma \cdot \varphi^T \cdot \dot{\varphi} + tr(\tilde{W}_0^T \cdot \Gamma_0^{-1} \cdot \dot{\tilde{W}}_0) + \gamma \cdot tr(\tilde{W}_1^T \cdot \Gamma_1^{-1} \cdot \dot{\tilde{W}}_1)$$

(3.67)

Introducing Eq. (3.55), Eq. (3.59), Eq. (3.64) and Eq. (3.65), we obtain:

$$\dot{L}_2 = r^T [-(V_m + K_v) r - K_u \cdot \varphi + \tilde{F}_0 + \gamma \cdot \tilde{F}_1] + \frac{1}{2} r^T \cdot \dot{M} \cdot r + \gamma \cdot \varphi^T \cdot (\tilde{F}_1 - K_u \cdot \varphi)$$

$$+ tr[\tilde{W}_0^T \cdot \Gamma_0^{-1} (-\Gamma_0 \cdot \sigma(V^T \cdot x) \cdot r^T + k \cdot \Gamma_0 \cdot \|\xi\| \cdot \hat{W}_0)]$$

$$+ \gamma \cdot tr[\tilde{W}_1^T \cdot \Gamma_1^{-1} (-\Gamma_1 \cdot \sigma_1(V^T \cdot y) \cdot \varphi^T - \Gamma_1 \cdot \sigma_1(V^T \cdot y) \cdot r^T + k \cdot \Gamma_1 \cdot \|\xi\| \cdot \hat{W}_1)]$$

$$= -r^T \cdot K_v \cdot r - r^T \cdot K_u \cdot \varphi + r^T \cdot \tilde{F}_0 + r^T \cdot \gamma \cdot \tilde{F}_1 + \frac{1}{2} r^T \cdot (\dot{M} - V_m) \cdot r$$

$$- \gamma \cdot \varphi^T \cdot K_u \cdot \varphi + \gamma \cdot \varphi^T \cdot \tilde{F}_1 + tr[-\tilde{W}_0^T \cdot \sigma(V^T \cdot x) \cdot r^T + \tilde{W}_0^T \cdot k \cdot \|\xi\| \cdot \hat{W}_0)]$$

$$+ \gamma \cdot tr[-\tilde{W}_1^T \cdot \sigma_1(V^T \cdot y) \cdot \varphi^T - \tilde{W}_1^T \cdot \sigma_1(V^T \cdot y) \cdot r^T + \tilde{W}_1^T \cdot k \cdot \|\xi\| \cdot \hat{W}_1)]$$

$$= -r^T \cdot K_v \cdot r - r^T \cdot K_u \cdot \varphi + r^T \cdot \tilde{F}_0 + r^T \cdot \gamma \cdot \tilde{F}_1 - \gamma \cdot \varphi^T \cdot K_u \cdot \varphi + \gamma \cdot \varphi^T \cdot \tilde{F}$$

$$- r^T \cdot \tilde{F}_0 - r^T \cdot \gamma \cdot \tilde{F}_1 - \gamma \cdot \varphi^T \cdot \tilde{F}_1 + tr(\tilde{W}_0^T \cdot k \cdot \|\xi\| \cdot \hat{W}_0) + \gamma \cdot tr(\tilde{W}_1^T \cdot k \cdot \|\xi\| \cdot \hat{W}_1)$$

$$= -r^T \cdot K_v \cdot r - r^T \cdot K_u \cdot \varphi + r^T \cdot (\varepsilon_0 + \varepsilon_1) - \gamma \cdot \varphi^T \cdot K_u \cdot \varphi + \gamma \cdot \varphi^T \cdot \varepsilon$$

$$+ tr(\tilde{W}_0^T \cdot k \cdot \|\xi\| \cdot \hat{W}_0) + \gamma \cdot tr(\tilde{W}_1^T \cdot k \cdot \|\xi\| \cdot \hat{W}_1)$$

Defining $Q = \begin{bmatrix} K_v & K_u \\ 0 & \gamma \cdot K_u \end{bmatrix}$ and $W = diag\{W_0 \quad \gamma \cdot W_1\}$, $\tilde{W} = W - \hat{W}$, we acquire:

$$\dot{L}_2 = -\xi^T \cdot Q \cdot \xi + r^T \cdot (\varepsilon_0 + \varepsilon_1) + \gamma \cdot \varphi^T \cdot \varepsilon_1 + k \cdot \|\xi\| \cdot tr(\tilde{W}^T \cdot W - \tilde{W}^T \cdot \tilde{W}) \tag{3.68}$$

Thus we have

$$\dot{L}_2 \le -\lambda \cdot \|\xi\|^2 + \|\xi\| \cdot \varepsilon_N + k \cdot \|\xi\| \cdot tr(\tilde{W}^T \cdot W - \|\tilde{W}^T\|_F^{\ 2})$$

$$\dot{L}_2 \le -\lambda \cdot \|\xi\|^2 + \|\xi\| \cdot \varepsilon_N + k \cdot \|\xi\| \cdot tr(\|\tilde{W}\|_F \cdot W_N - \|\tilde{W}\|_F^{\ 2}) \tag{3.69}$$

where $\lambda_{Q\min}$ is the minimum eigenvalue of Q and $\varepsilon_N = \max(|\varepsilon_0 + \varepsilon_1| \quad \gamma \cdot |\varepsilon_1|)$, W_N is the bound of the ideal weight matrix W,

And $$tr(\|\tilde{W}\|_F \cdot W_N - \|\tilde{W}\|_F^2) \le \|\tilde{W}\|_F \cdot W_N - \|\tilde{W}\|_F^2.$$

We have

$$\dot{L}_2 \le -\lambda_{Q\min} \cdot \|\xi\|^2 + \|\xi\| \cdot \varepsilon_N + k \cdot \|\xi\| \cdot (\|\tilde{W}\|_F \cdot W_N - \|\tilde{W}\|_F^2)$$

$$\dot{L}_2 \le -\|\xi\| \cdot [\lambda_{Q\min} \cdot \|\xi\| - \varepsilon_N - k \cdot (\|\tilde{W}\|_F \cdot W_N - \|\tilde{W}\|_F^2)]$$

and $$\lambda_{Q\min} \cdot \|\xi\| - \varepsilon_N - k \cdot (\|\tilde{W}\|_F \cdot W_N - \|\tilde{W}\|_F^2)$$

$$= \lambda_{Q\min} \cdot \|\xi\| - \varepsilon_N - \frac{k \cdot W_N^2}{4} + k \cdot (\|\tilde{W}\|_F - \frac{W_N}{2})^2$$

If we have

$$\lambda_{Q\min} \cdot \|\xi\| - \varepsilon_N - \frac{k \cdot W_N^2}{4} > 0$$

$$\|\xi\| > \frac{k \cdot W_N^2/4 + \varepsilon_N}{\lambda_{Q\min}} \tag{3.70}$$

or

$$\|\tilde{W}\|_F > W_N/2 + \sqrt{W_N^2/4 + \varepsilon_N/k} \tag{3.71}$$

, we can prove $\dot{L}_2$ negative. Inequality (3.71) shows that if the control gains K_f, K_v, and K_u are chosen large enough so that

$$\frac{k \cdot W_N^2/4 + \varepsilon_N}{\lambda_{Q\min}} < b_\xi$$

where $b_\xi > 0$ represents the radius of a ball inside the compact set C_ξ of filtered error $\xi(t)$.

Thus, any trajectory $\xi(t)$ starting in compact set $C_\xi = \{\xi | \|\xi\| \le b_\xi\}$ converges within C_ξ and is bounded. According to the standard Lyapunov theorem extension [45], it demonstrates the UUB (uniformly ultimately bounded) of both $\xi(t)$ and $\widetilde{W}$.

The overall NN controller structure is shown as Fig. 3.1. The control algorithm is summarized as the following steps.

Step i With Eq. (3.17), and Eq. (3.18), the filtered error $r(t)$ is obtained.

Step ii Following the control strategy Eq. (3.41), the control signal $\tau_0(t)$ is calculated.

Step iii The fictitious variable $\varphi(t)$ is obtained by Eq. (3.56).

Step iv Following the control strategy Eq. (3.54), control signal $\tau_1(t)$ is computed.

Step v The overall control signal $\tau(t)$ is calculated using the control scheme Eq. (3.19), Eq. (3.20), and Eq. (3.35).

3.5 Conclusion

The dynamic model of RLFJ robot manipulator is decomposed into two different scale models by integral manifold theory. The control objects are also defined. In the proposed adaptive NN controller, which is designed for a RLFJ robot manipulator with unknown nonlinearities, two NNs are used to approximate two complicated unknown nonlinear functions in both fast and slow control components. No off-line training is required for NNs. The control algorithm and the weight matrix update rule are derived from Lyapunov theorem extension. The stability and the boundedness of tracking error of this unknown RLFJ robot manipulator have been proved. Simulation results in chapter 4

show that the proposed NN controller outperforms the adaptive composite control method and can be applicable to unknown flexible robots with a larger range of stiffness.

Chapter 4 Simulation results

In this chapter, the effectiveness of the proposed control scheme is demonstrated on a two-link RLFJ robot manipulator, which can be described in the form of Eq. (3.14a) and Eq. (3.14b), in which

$$M(q)=\begin{bmatrix} a+b\cdot\cos(q_2) & c+\frac{b}{2}\cdot\cos(q_2) \\ c+\frac{b}{2}\cdot\cos(q_2) & c \end{bmatrix}$$

$$V_m(q,\dot{q})=\begin{bmatrix} -\frac{b}{2}\cdot\dot{q}_2\cdot\sin(q_2) & -\frac{b}{2}\cdot(\dot{q}_1+\dot{q}_2)\cdot\sin(q_2) \\ \frac{b}{2}\cdot\dot{q}_1\cdot\sin(q_2) & 0 \end{bmatrix}$$

$$G(q)=\begin{bmatrix} d\cdot\cos(q_1)+e\cdot\cos(q_2) \\ e\cdot\cos(q_1+q_2) \end{bmatrix}$$

$$F(\dot{q})=\begin{bmatrix} \{35+1.1\cdot e^{-50|\dot{q}_1|}+0.9(1-e^{-65|\dot{q}_1|})\}\cdot\mathrm{sgn}(\dot{q}_1) \\ \{38+1.0\cdot e^{-55|\dot{q}_2|}+0.95(1-e^{-60|\dot{q}_2|})\}\cdot\mathrm{sgn}(\dot{q}_2) \end{bmatrix}$$

$$a=l_2^{\,2}\cdot m_2+l_1^{\,2}\cdot(m_1+m_2),\quad b=2\cdot l_1\cdot l_2\cdot m_2,\quad c=l_2^{\,2}\cdot m_2$$

$$d=(m_1+m_2)\cdot l_1\cdot g_0,\quad e=m_2\cdot l_2\cdot g_0$$

The parameter values are shown in Table 4-1.

Table 4-1 Parameter values of RLFJ system

System Parameters	Values
Link 1 length (m)	1
Link 2 length (m)	1
Mass of link 1 (kg)	0.8
Mass of link 2(kg)	2.3
Gravity acceleration (m/s2)	9.8

4.1 Control performance of rigid case

Assuming the elastic coefficient $\gamma = 0$, the dynamic model of rigid joint robot manipulator is given by Eq. (3.21). The inputs to the NNs are given by

$$x = \begin{bmatrix} \ddot{q}^T & \dot{q}^T & q^T & \ddot{q}_d{}^T & \dot{q}_d{}^T & \text{sgn}(\dot{q})^T & 1 \end{bmatrix}^T$$

$$y = \begin{bmatrix} \tau_0{}^T & q^T & \dot{q}^T & \ddot{q}^T & 1 \end{bmatrix}^T$$

Two input reference signal are chosen as desired two joints positions: $q_{1d} = 2 \cdot \sin(0.1\pi \cdot t)$ and $q_{2d} = 3 \cdot \sin(0.1\pi \cdot t)$. The control objective is defined as to make the rigid joint robot joint angle $q = [q_1 \quad q_2]^T$ follow the given desired joint trajectory $q_d = [q_{1d} \quad q_{2d}]^T$. The gains are selected as: $\Lambda = [20 \quad 1]^T$, $K_V = diag\{50 \quad 50\}$, $\Gamma_0 = diag\{10 \quad 10\}$, and $k = 0.1$. The system responses under the control of the proposed NN-based controller are shown in Fig. 4-1.

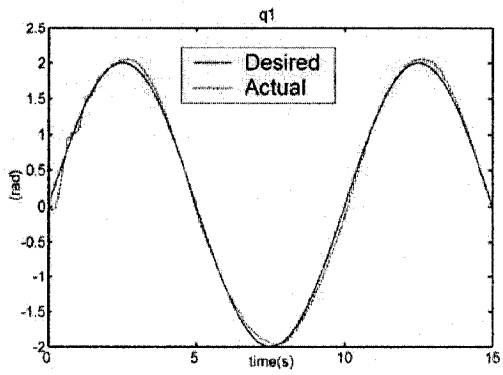

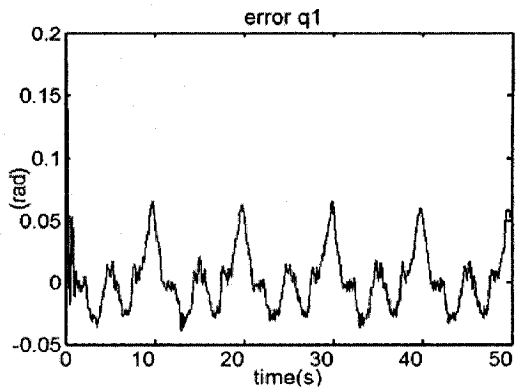

(*a*) (*b*)

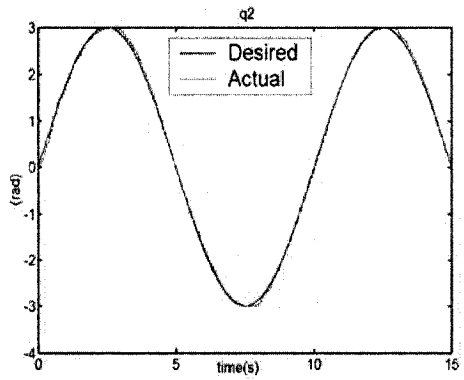

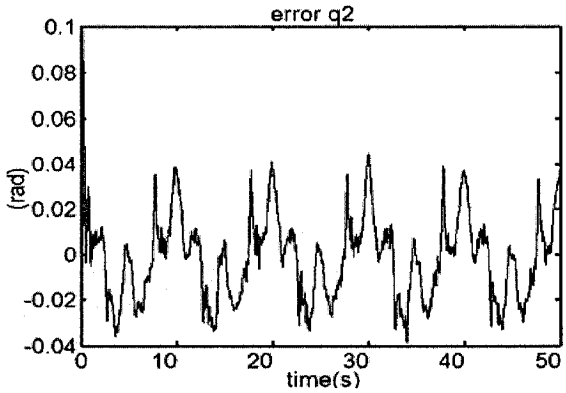

(*c*) (*d*)

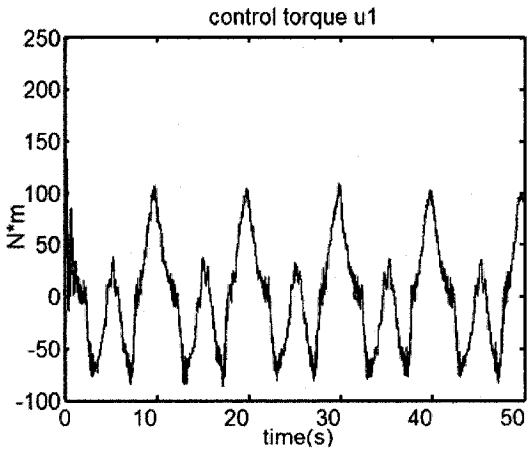

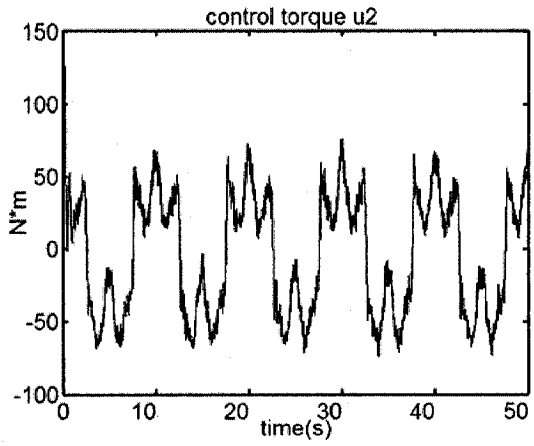

(*e*) (*f*)

Figure 4-1 Performance of NN controller with $\gamma = 0$, $K = diag\{100 \quad 100\}$

(a) Actual (dashed line) and desired (solid) joint q_1 angles (b) Error $q_1 - q_{1d}$

(c) Actual (dashed line) and desired (solid) joint q_2 angles. (d) Error $q_2 - q_{2d}$,

(e) Bounded control torque of joint u_1 (f) Bounded control torque u_2

4.2 Control performance of flexible case

The flexible joint parameters are $J = diag\{0.3 \quad 0.3\}$, $B = diag\{0.02 \quad 0.02\}$, $K = diag\{100 \quad 100\}$. The inputs to the NNs are given by

$$x = \left[\ddot{q}^T \quad \dot{q}^T \quad q^T \quad \ddot{q}_d{}^T \quad \dot{q}_d{}^T \quad \text{sgn}(\dot{q})^T \quad 1\right]^T$$

$$y = \left[\tau_0{}^T \quad q^T \quad \dot{q}^T \quad \ddot{q}^T \quad 1\right]^T$$

Two input reference signal are chosen as desired two joints positions: $q_{1d} = 2 \cdot \sin(0.1\pi \cdot t)$ and $q_{2d} = 3 \cdot \sin(0.1\pi \cdot t)$. The control objective is defined as to make the flexible-joint robot joint angle $q = [q_1 \quad q_2]^T$ follow the given desired joint trajectory $q_d = [q_{1d} \quad q_{2d}]^T$. The gains are selected as: $\Lambda = [20 \quad 1]^T$, $K_V = diag\{50 \quad 50\}$, $K_u = diag\{5 \quad 5\}$, $K_f = diag\{3 \quad 3\}$, $\Gamma_0 = diag\{10 \quad 10\}$, $\Gamma_1 = diag\{20 \quad 20\}$, and $k = 0.1$. The system responses under the control of the proposed NN-based controller are shown in Fig. 4-2.

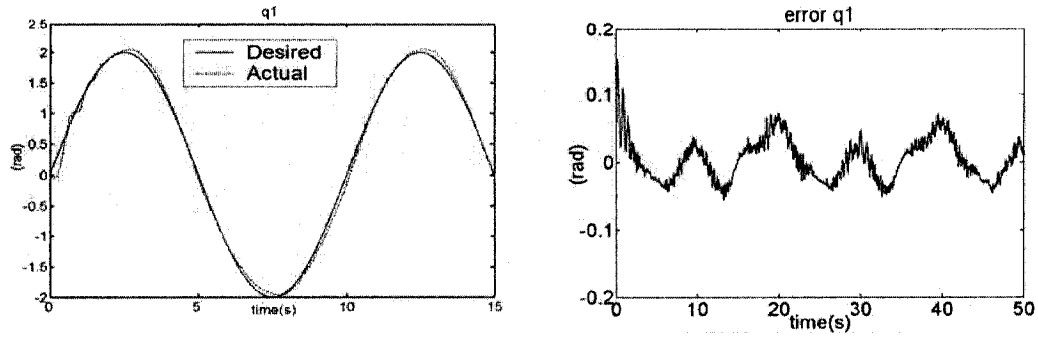

(*a*) (*b*)

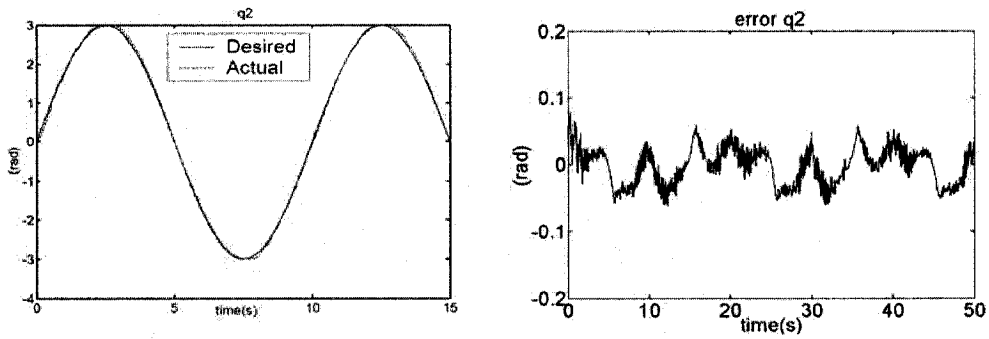

(*c*) (*d*)

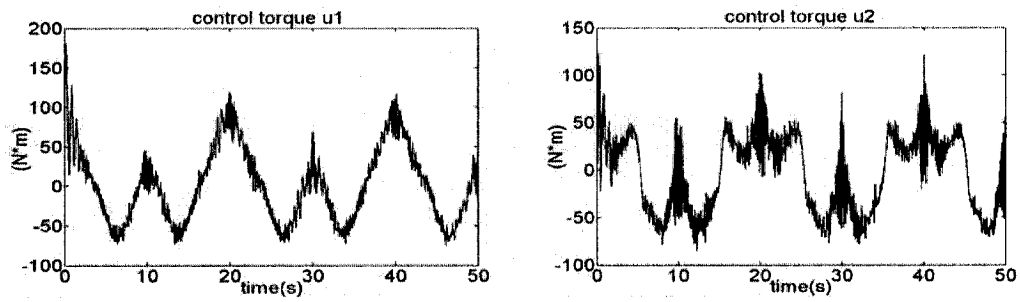

(*e*) (*f*)

Figure 4-2 Performance of NN controller with $K = diag\{100 \quad 100\}$

(a) Actual (dashed line) and desired (solid) joint q_1 angles (b) Error $q_1 - q_{1d}$

(c) Actual (dashed line) and desired (solid) joint q_2 angles. (d) Error $q_2 - q_{2d}$,

(e) Bounded control torque of joint u_1 (f) Bounded control torque u_2

For a comparison of performance, we have implemented the adaptive manifold scheme [23] by using the same control parameters. The simulation results are shown in Fig. 4-3. Please note that an unknown friction term is added in the robot model, which makes the control problem more challenging than that in [23].

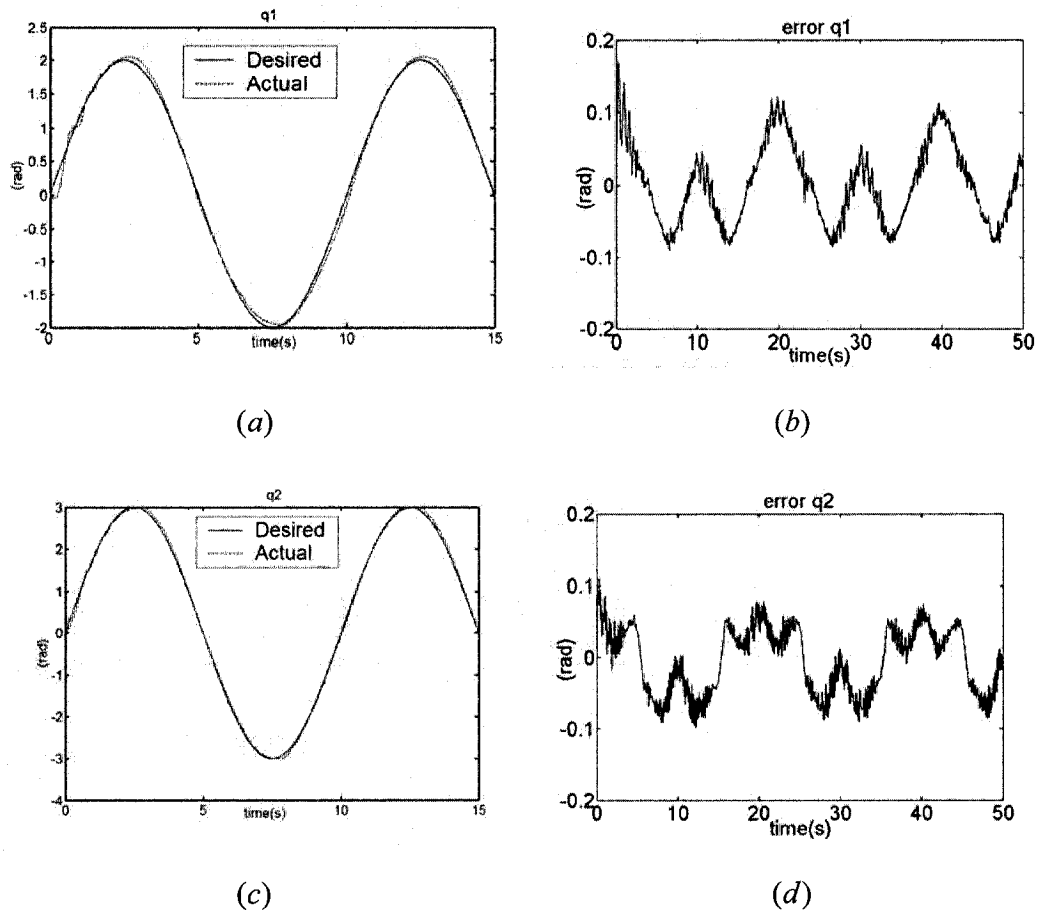

Figure 4-3 Performance of adaptive integral manifold scheme [23]

(a) Actual (dashed line) and desired (solid line) joint q_1 angles (b) Error $q_1 - q_{1d}$

(c) Actual (dashed line) and desired (solid line) joint q_2 angles (d) Error $q_2 - q_{2d}$

The simulation results show that the proposed NN-based controller outperforms the adaptive manifold approach with simpler implementation. The NN is tuned on-line without any preliminary off-line training.

4.3 Robustness test

In order to test the robustness of the controller, we change the system parameters to $l_1 = 1.2m, \quad l_2 = 0.8m, \quad m_1 = 1kg, \quad m_2 = 2kg$ and apply the same NN-based controller to the system. The system responses are shown in Fig. 4-4.

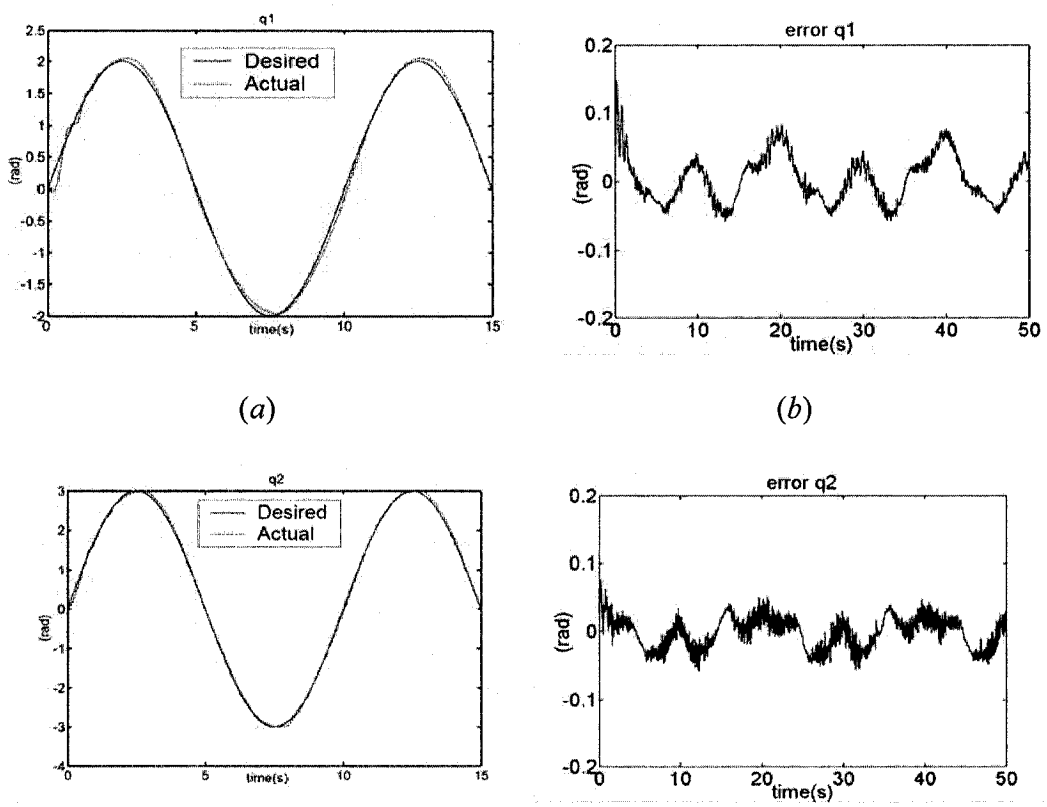

Figure 4-4 Performance of adaptive integral manifold scheme [23] controller with 20% change of system parameters

(a) Actual (dashed line) and desired (solid line) joint q_1 angles (b) Error $q_1 - q_{1d}$

(c) Actual (dashed line) and desired (solid line) joint q_2 angles (d) Error $q_2 - q_{2d}$

For a comparison of performance, we still change the system parameters to $l_1 = 1.2m$, $l_2 = 0.8m$, $m_1 = 1kg$, $m_2 = 2kg$ and implemented the same adaptive manifold scheme [23]. The system responses are shown in Fig. 4-5.

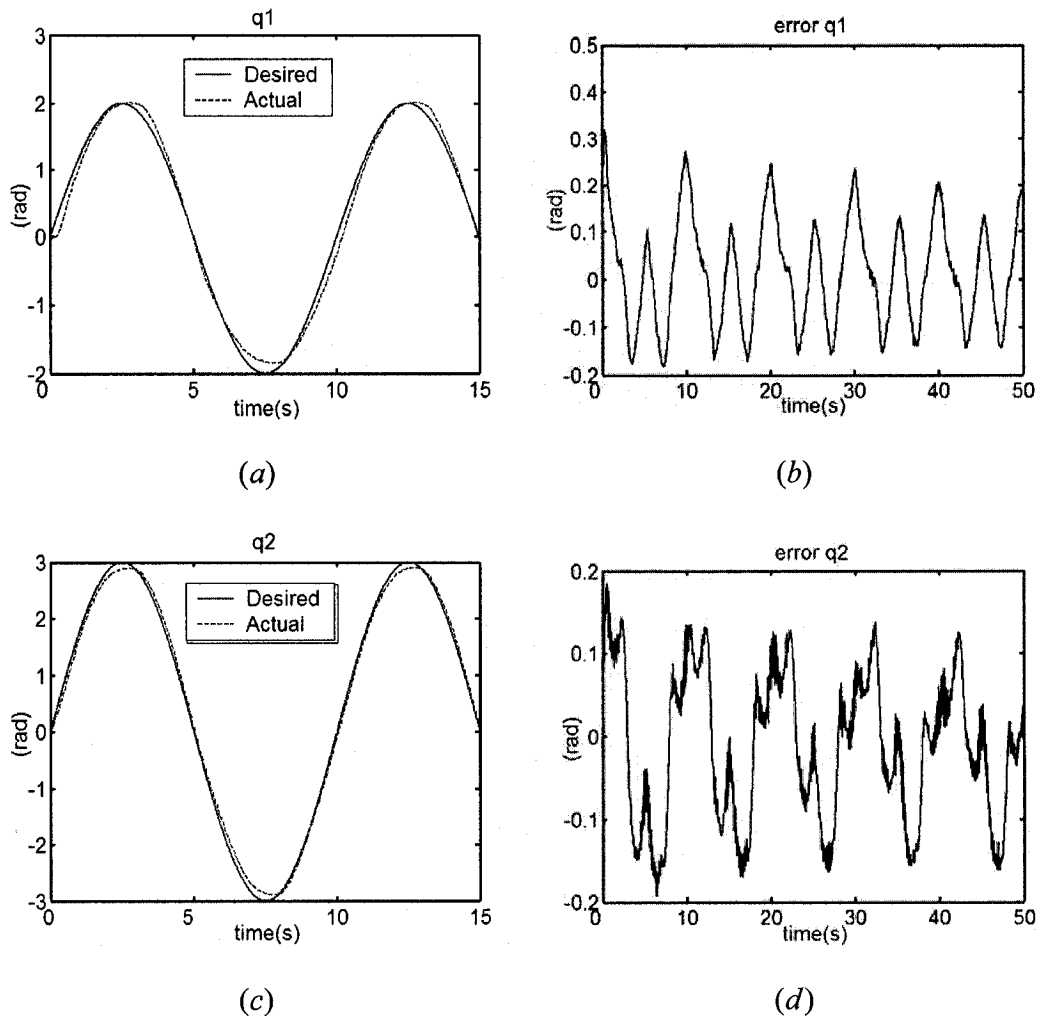

Figure 4-5 Performance of adaptive integral manifold scheme [23] controller with 20% change of system parameters

(a) Actual (dashed line) and desired (solid line) joint q_1 angles (b) Error $q_1 - q_{1d}$

(c) Actual (dashed line) and desired (solid line) joint q_2 angles (d) Error $q_2 - q_{2d}$

From the above results, we observe that the proposed NN controlled system gives a

good response when the system parameters are changed within 20% percent range. The test results show that the NN controller owns the ability to deal with the system uncertainties.

4.4 Stiffness parameter

Further simulation runs have been carried out to test the effect of stiffness variation to the controller. We run the same controller using two stiffness parameters: $K = diag\{300 \quad 300\}$ and $K = diag\{30 \quad 30\}$. The system responses are shown in Fig. 4-6 and 4-7. The results demonstrate that the proposed controller can deal with relative large range stiffness change.

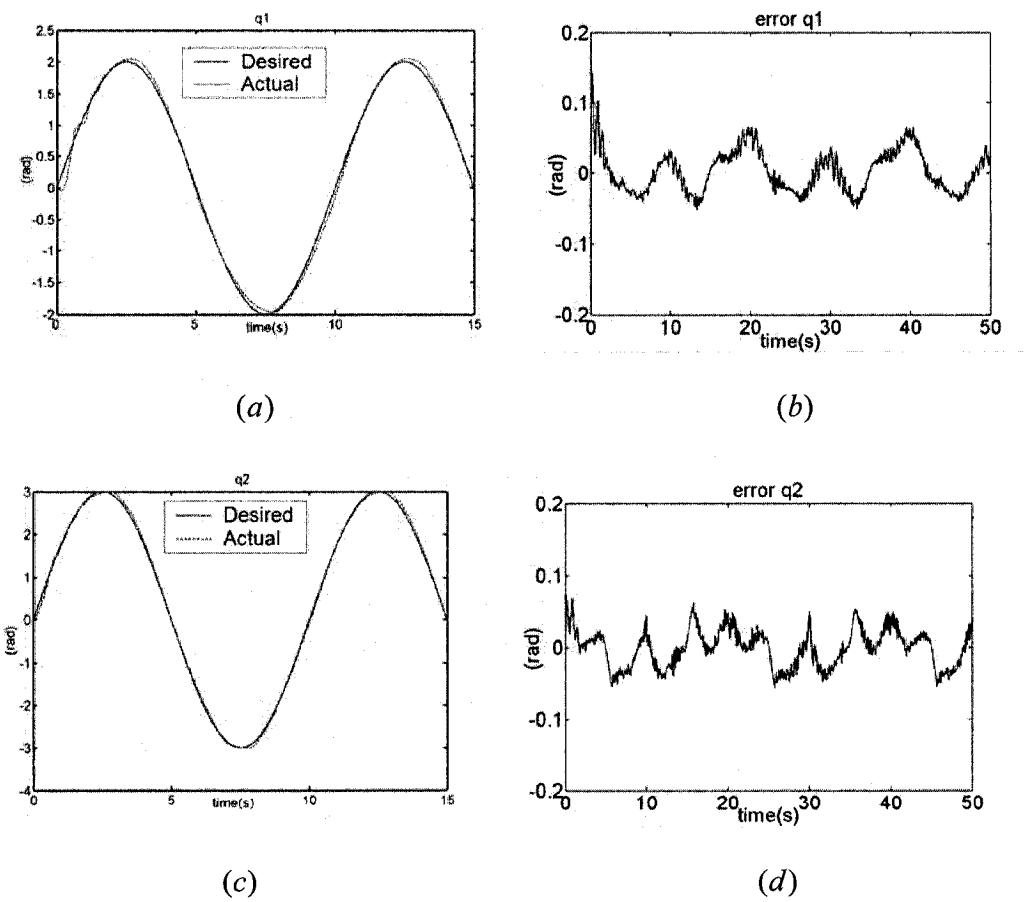

Figure 4-6 Performance of NN controller with stiffness parameters $K = diag\{300 \quad 300\}$

(a) Actual (dashed line) and desired (solid line) joint q_1 angles (b) Error $q_1 - q_{1d}$

(c) Actual (dashed line) and desired (solid line) joint q_2 angles (d) Error $q_2 - q_{2d}$

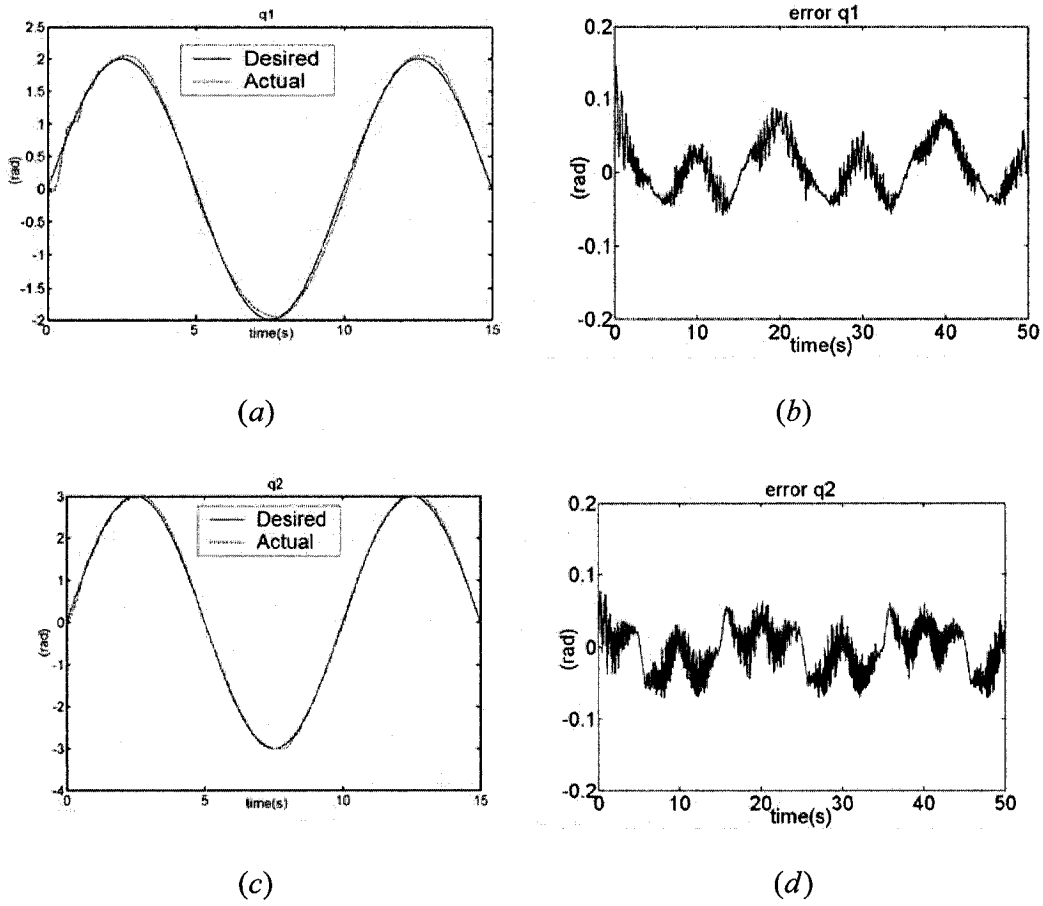

Figure 4-7 Performance of NN controller with stiffness parameters $K = diag\{30 \quad 30\}$

(a) Actual (dashed line) and desired (solid line) joint q_1 angles (b) Error $q_1 - q_{1d}$

(c) Actual (dashed line) and desired (solid line) joint q_2 angles (d) Error $q_2 - q_{2d}$

4.5 Conclusion

Fig. 4-1--4-7 shows the simulation results of applying the NN controller to RLFJ system for tracking desired signal. We can see that a very good tracking performance is obtained. The NN controller can indeed improve the tracking performance without resorting to high-gain feedback. In addition, we do not even need to know the explicit parameters of system. Moreover, the NN controller can be implemented in a wide stiffness parameter range. This is a significant advantage since the NN controller can be applied to any type of flexible or rigid robots with little modification to gain parameters.

Chapter 5 NN based Adaptive Compensator Design for unknown Hysteresis

With the increasing usage of piezoelectric actuators in precision machining, many researches have been focused on the compensator design based on various hysteresis models since it is an unavoidable nonlinearities of these actuators. In this chapter, an NN based adaptive compensator is proposed for a piezoelectric actuator with unknown hysteresis. By analyzing the solution of the differential dynamic model of hysteresis [58, 59], which is described by Duhem model, a dynamic pre-inversion compensator is built to cancel the effect of the hysteresis.

5.1 General Duhem model

Many different mathematic models are built to describe the hysteresis behaviours such as: Preisach model, Prandtl-Ishlinkii model, Duhem model. Among these, the Duhem model and Preisach model are most popular in recent research because both of them are capable of representing many forms of hysteresis and mathematically tractable for design control. Considering its capability to provide a finite-dimensional differential model of hysteresis [58,59], this thesis will adopt classical Duhem model in a piezoelectric actuator. Some important properties of the Duhem model are also introduced in this Section.

As shown in Figure 5-1, τ_{pr} is the actuator output, τ_{pd} is the control input.

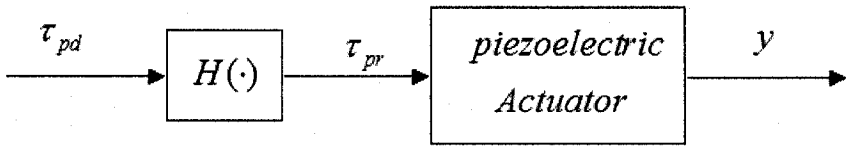

Figure 5-1: Piezoelectric actuator with hysteresis

The Duhem model is used to describe hysteresis $H(t)$, which appears in piezoelectric actuator, by the following mathematical model as shown in Figure 5-2

$$\frac{d\tau_{pr}}{dt} = \alpha \cdot \left|\frac{dv}{dt}\right| \cdot [f(v) - \tau_{pr}] + \frac{dv}{dt} \cdot g(v) \tag{5.1}$$

or it can be write as

$$\frac{d\tau_{pr}}{dv} = \begin{cases} \alpha \cdot [f(v) - \tau_{pr}] + g(v), & \dot{v} > 0 \\ -\alpha \cdot [f(v) - \tau_{pr}] + g(v), & \dot{v} < 0 \end{cases} \tag{5.2}$$

where α is positive number.

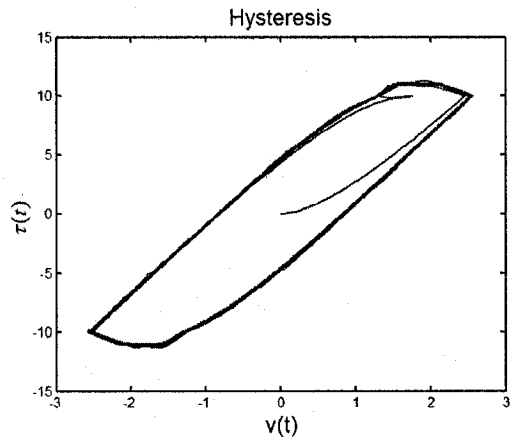

Figure 5-2: Duhem hysteresis model

The Duhem model is a rate independent operator, with input signal $v, \dot{v}$ and output signal τ_{pr}. In Eq. (5.2), $g(v)$ can be defined as the slope of the model, and $f(v)$ can be defined as the average value of the different between upward side and downward side.

Property 5.1: $f(v)$ is a piecewise continuous, monotone increasing, odd function with a derivative $f'(v)$, that is not identically zero. For large value of input $v(t)$, there exist a finite limit $f'(\infty)$;

$$f(v) = -f(-v), \ \lim_{v \to \infty} f'(v) < \infty \tag{5.3}$$

Property 5.2: $g(v)$ is a piecewise continuous, even function with limiting $g'(\infty)$ for large value of input $v(t)$,

$$g(v) = g(-v), \ \lim_{v \to \infty} g'(v) < \infty \tag{5.4}$$

It's has been shown that Duhem model can describe a large class of hysteresis in varies materials, such as magnetic, shape memory alloy, which are unavoidable in actuator. One widely used pair of functions of $f(v)$ and $g(v)$ are

$$f(v) = \begin{cases} a_1 \cdot v_s + a_2(v - v_s) & for \quad v > v_s \\ a_1 \cdot v & for \quad |v| \le v_s \\ -a_1 \cdot v_s + a_2(v + v_s) & for \quad v < -v_s \end{cases} \tag{5.5}$$

$$g(v) = a_3 \tag{5.6}$$

with $v_s > 0$, $a_1 > 0$, $a_2 > 0$, $1 > a_3 > 0$

Introducing Eq. (5.5) and Eq. (5.6) into Eq. (5.1), we have

$$\dot{\tau}_{pr} = \begin{cases} \alpha \cdot \dot{v}[a_1 \cdot v_s + a_2(v - v_s) - \tau_{pr}] + a_3 \cdot \dot{v} & \dot{v} \geq 0 \quad and \quad v > v_s \\ \alpha \cdot \dot{v}[a_1 \cdot v - \tau_{pr}] + a_3 \cdot \dot{v} & \dot{v} \geq 0 \quad and \quad |v| \leq v_s \\ \alpha \cdot \dot{v}[-a_1 \cdot v_s + a_2(v + v_s) - \tau_{pr}] + a_3 \cdot \dot{v} & \dot{v} \geq 0 \quad and \quad v < -v_s \\ -\alpha \cdot \dot{v}[\tau_{pr} - a_1 \cdot v_s - a_2(v - v_s)] + a_3 \cdot \dot{v} & \dot{v} < 0 \quad and \quad v > v_s \\ -\alpha \cdot \dot{v}[\tau_{pr} - a_1 \cdot v] + a_3 \cdot \dot{v} & \dot{v} < 0 \quad and \quad |v| \leq v_s \\ -\alpha \cdot \dot{v}[\tau_{pr} + a_1 \cdot v_s - a_2(v + v_s)] + a_3 \cdot \dot{v} & \dot{v} < 0 \quad and \quad v < -v_s \end{cases} \tag{5.7}$$

Eq. (5.7) can be solved for τ_{pr}

$$\tau_{pr} = \begin{cases} a_2 \cdot v - f_{21} & \dot{v} \geq 0 \quad and \quad v > v_s \\ a_1 \cdot v - f_{22} & \dot{v} \geq 0 \quad and \quad |v| \leq v_s \\ a_2 \cdot v - f_{23} & \dot{v} \geq 0 \quad and \quad v < -v_s \\ a_2 \cdot v - f_{24} & \dot{v} < 0 \quad and \quad v > v_s \\ a_1 \cdot v - f_{25} & \dot{v} < 0 \quad and \quad |v| \leq v_s \\ a_2 \cdot v - f_{26} & \dot{v} < 0 \quad and \quad v < -v_s \end{cases} \tag{5.8}$$

with

$$\begin{cases} f_{21} = (a_2 \cdot v_0 - \tau_{pr0}) \cdot e^{-\alpha(v - v_0)} - e^{-\alpha \cdot v} \int_{v_0}^{v} (a_3 - a_2) \cdot e^{\alpha \cdot \zeta} d\zeta - (a_1 - a_2) \cdot v_s & \dot{v} \geq 0 \quad and \quad v > v_s \\ f_{22} = (a_1 \cdot v_0 - \tau_{pr0}) \cdot e^{-\alpha(v - v_0)} - e^{-\alpha \cdot v} \int_{v_0}^{v} (a_3 - a_1) \cdot e^{\alpha \cdot \zeta} d\zeta & \dot{v} \geq 0 \quad and \quad |v| \leq v_s \\ f_{23} = (a_2 \cdot v_0 - \tau_{pr0}) \cdot e^{-\alpha(v - v_0)} - e^{-\alpha \cdot v} \int_{v_0}^{v} (a_3 - a_2) \cdot e^{\alpha \cdot \zeta} d\zeta + (a_1 - a_2) \cdot v_s & \dot{v} \geq 0 \quad and \quad v < -v_s \\ f_{24} = (a_2 \cdot v_0 - \tau_{pr0}) \cdot e^{\alpha(v - v_0)} - e^{\alpha \cdot v} \int_{v_0}^{v} (a_3 - a_2) \cdot e^{-\alpha \cdot \zeta} d\zeta - (a_1 - a_2) \cdot v_s & \dot{v} < 0 \quad and \quad v > v_s \\ f_{25} = (a_1 \cdot v_0 - \tau_{pr0}) \cdot e^{\alpha(v - v_0)} - e^{\alpha \cdot v} \int_{v_0}^{v} (a_3 - a_1) \cdot e^{-\alpha \cdot \zeta} d\zeta & \dot{v} < 0 \quad and \quad |v| \leq v_s \\ f_{26} = (a_2 \cdot v_0 - \tau_{pr0}) \cdot e^{\alpha(v - v_0)} - e^{\alpha \cdot v} \int_{v_0}^{v} (a_3 - a_2) \cdot e^{-\alpha \cdot \zeta} d\zeta + (a_1 - a_2) \cdot v_s & \dot{v} < 0 \quad and \quad v < -v_s \end{cases} \tag{5.9}$$

which is a complex nonlinear function.

$$\tau_{pr} = (a_1 \cdot \chi_1 + a_2 \cdot \chi_2) \cdot v$$

$$-(f_{21}\cdot\chi_1\cdot\chi_3+f_{22}\cdot\chi_1\cdot\chi_4+f_{23}\cdot\chi_1\cdot\chi_5+f_{24}\cdot\chi_2\cdot\chi_3+f_{25}\cdot\chi_2\cdot\chi_4+f_{26}\cdot\chi_2\cdot\chi_5)$$

(5.10)

where χ is a indicator functions: $\chi_1=\begin{cases}1 & \dot{v}\geq 0\\ 0 & \dot{v}<0\end{cases}$, $\chi_2=\begin{cases}0 & \dot{v}\geq 0\\ 1 & \dot{v}<0\end{cases}$, $\chi_3=\begin{cases}1 & v>v_s\\ 0 & v\leq 0\end{cases}$,

$\chi_4=\begin{cases}1 & |v|\leq v_s\\ 0 & |v|>v_s\end{cases}$, $\chi_5=\begin{cases}1 & v<-v_s\\ 0 & v\geq -v_s\end{cases}$

Following the definition of the indicator functions, we get

$$\chi_1\cdot\chi_2=0,\ \chi_1+\chi_2=1,\chi_3\cdot\chi_4\cdot\chi_5=0,\ \chi_3+\chi_4+\chi_5=1,\ \chi_k^{\ 2}=\chi_k \tag{5.11}$$

By defining $\dot{\chi}_1=\dot{\chi}_2=\dot{\chi}_3=\dot{\chi}_4=\dot{\chi}_5=0$, we have

$$\dot{\tau}_{pr}=(a_1\cdot\chi_1+a_2\cdot\chi_2)\cdot\dot{v}$$

$$-(\dot{f}_{21}\cdot\chi_1\cdot\chi_3+\dot{f}_{22}\cdot\chi_1\cdot\chi_4+\dot{f}_{23}\cdot\chi_1\cdot\chi_5+\dot{f}_{24}\cdot\chi_2\cdot\chi_3+\dot{f}_{25}\cdot\chi_2\cdot\chi_4+\dot{f}_{26}\cdot\chi_2\cdot\chi_5)$$

(5.12)

Remark 5.1: From the definition of χ_k, the indicator function is a step function, which jump between 2 values: 0 and 1. As a result, $\dot{\chi}_k=0$ except those jump points, at which $\dot{\chi}_k\to\pm\infty$. For convenience, we set $\dot{\chi}_k=0$ at these jump points. Actually, the updating rule for the NN controller is stopped in these skip-point and all the parameters are kept as the last updating values. That is to say, when controller works under those conditions, it will skip those time steps.

5.2 Control Objective

In order to eliminate the effect of hysteresis to the whole piezoelectric actuator

system, an NN based hysteresis compensator is design to make the real control signal τ_{pr} approach the desired control signal τ_{pd}. Figure 5-3 shows a schematic of inverse control, where $H(\cdot)$ represents the Duhem model. The input to $H(\cdot)$ is obtained through inversion of $HI(\cdot)$. The goal of the hysteresis inverse function is to guarantee the integrated system stability make the error between the reference trajectory τ_{pd} and the achieved trajectory τ_{pr} approach zero.

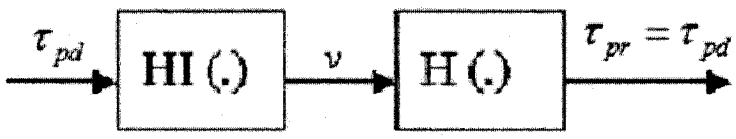

Figure 5-3: Structure of hysteresis compensator

5.3 Compensator design for Hysteresis

In presence of the unknown hysteresis nonlinearity, the desired control signal τ_{pr} for the piezoelectric actuator is different with the real control signal τ_{pd}. Define their error as

$$\tilde{\tau}_{pr} = \tau_{pd} - \tau_{pr} \tag{5.13}$$

Differentiate Eq. (5.13), yielding

$$\dot{\tilde{\tau}}_{pr} = \dot{\tau}_{pd} - \dot{\tau}_{pr} \tag{5.14}$$

With Eq. (5.12), we have

$$\dot{\tilde{\tau}}_{pr} = \dot{\tau}_{pd} - K_a \cdot \dot{v} + F_2 \tag{5.15}$$

where $F_2 = \dot{f}_{21} \cdot \chi_1 \cdot \chi_3 + \dot{f}_{22} \cdot \chi_1 \cdot \chi_4 + \dot{f}_{23} \cdot \chi_1 \cdot \chi_5 + \dot{f}_{24} \cdot \chi_2 \cdot \chi_3 + \dot{f}_{25} \cdot \chi_2 \cdot \chi_4 + \dot{f}_{26} \cdot \chi_2 \cdot \chi_5$, and $K_a = a_1 \cdot \chi_1 + a_2 \cdot \chi_2$

Again, we utilize a second first-layer-fixed MLP to approximate the nonlinear function F_2.

$$F_2 = W_2^T \cdot \sigma(V_2^T \cdot h) + W_{f21}^T \cdot \varphi_{21}[V_{f21}^T \cdot (h - c_{21})]$$
$$+ W_{f22}^T \cdot \varphi_{22}[V_{f22}^T \cdot (h - c_{22})] + W_{f23}^T \cdot \varphi_{23}[V_{f23}^T \cdot (h - c_{23})] + \varepsilon_2(h) \qquad (5.16)$$

where $h = [\tau_{pd} \quad \tau_{p0} \quad v \quad \dot{v} \quad 1]^T$, τ_{p0} is the initial value of the control signal, V_2^T, V_{f21}^T, V_{f22}^T, and V_{f23}^T are input-layer weight matrix, W_2^T, W_{f21}^T, W_{f22}^T, and W_{f22}^T are output-layer weight matrix, c_{21}, c_{22}, and c_{23} are jump points, and $\sigma(\cdot)$, $\varphi_{21}(\cdot)$, $\varphi_{21}(\cdot)$, and $\varphi_{23}(\cdot)$ are the activation functions. Output-layer weight matrix W_2^T, W_{f21}^T, W_{f22}^T, and W_{f23}^T are trained the same way, including threshold weights. Weights V_2^T, V_{f21}^T, V_{f22}^T, V_{f23}^T and threshold c_{21}, c_{22}, c_{23} are fixed.

To construct a reasonable hysteresis model, the following properties will be utilized:

Property 5.3: There exist known constant $a_{\min}$ and $a_{\max}$, such that a_1 and a_2 satisfy $a_1, a_2 \in [a_{\min} \quad a_{\max}]$.

Property 5.4: Unknown nonlinear function F_2 is bounded by a known constant $\|f_2\| \le B$.

Then, design a compensator as the Figure 5-4 shown

$$\dot{v} = \hat{\mu} \cdot \{k_b \cdot \tilde{\tau}_{pr} + \dot{\tau}_{pd} + \hat{W}_2^T \cdot \sigma_2(V^T \cdot h) + \hat{W}_{f21}^T \cdot \varphi_{21}(V_{f21}^T \cdot h)$$
$$+ \hat{W}_{f22}^T \cdot \varphi_{22}[V_{f22}^T \cdot (h - v_s)] + \hat{W}_{f23}^T \cdot \varphi_{23}[V_{f23}^T \cdot (h + v_s)]\} \qquad (5.17)$$

where $\hat{\mu} = \frac{a_{\min}^2}{\hat{a}_1 \cdot \hat{a}_2}$ is an estimated constant, which satisfy $0 < \hat{\mu} \leq 1$ with the known boundary of $a_1, a_2 \in [a_{\min} \quad a_{\max}]$, k_b is a positive constant, $\hat{a}_1$, $\hat{a}_2$ is the estimated value of a_1, a_2 and $\hat{W}_2^T$, $\hat{W}_{f21}^T$, $\hat{W}_{f22}^T$, and $\hat{W}_{f23}^T$ are the estimated output-layer weight matrix W_2^T, W_{f21}^T, W_{f22}^T, and W_{f23}^T.

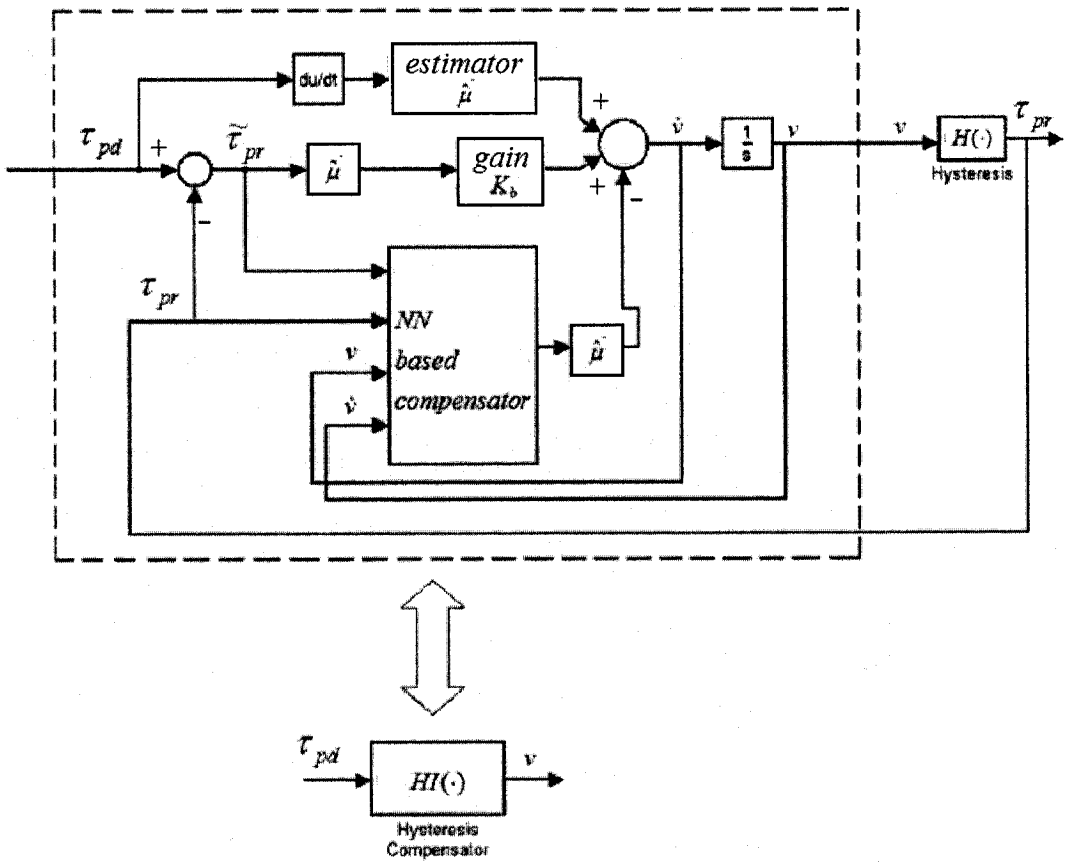

Figure 5-4 Hysteresis compensator structure

Introducing Eq. (5.16), Eq. (5.17) into Eq. (5.15), we get

$$\dot{\tilde{\tau}}_{pr} = -k_b \cdot \hat{\mu} \cdot K_a \cdot \tilde{\tau}_{pr} + (1 - \hat{\mu} \cdot K_a) \cdot \dot{\tau}_{pd} + (1 - \hat{\mu} \cdot K_a) \cdot \hat{W}_2^T \cdot \sigma(V^T \cdot h) + \tilde{W}_2^T \cdot \sigma(V^T \cdot h)$$

$$+(1-\hat{\mu}\cdot K_a)\cdot\{\hat{W}_{f21}{}^T\cdot\varphi_{22}(V_{f22}{}^T\cdot h)+\hat{W}_{f22}{}^T\cdot\varphi_{22}[V_{f22}{}^T\cdot(h-v_s)]+\hat{W}_{f23}{}^T\cdot\varphi_{23}[V_{f23}{}^T\cdot(h+v_s)]\}$$

$$+\tilde{W}_{f21}{}^T\cdot\varphi_{21}(V_{f21}{}^T\cdot h)+\tilde{W}_{f22}{}^T\cdot\varphi_{22}[V_{f22}{}^T\cdot(h-v_s)]+\tilde{W}_{f23}{}^T\cdot\varphi_{23}[V_{f23}{}^T\cdot(h+v_s)]+\varepsilon_2(h) \tag{5.18}$$

where
$$\tilde{W}_2{}^T=W_2{}^T-\hat{W}_2{}^T \tag{5.19a}$$

$$\tilde{W}_{f21}{}^T=W_{f21}{}^T-\hat{W}_{f21}{}^T \tag{5.19b}$$

$$\tilde{W}_{f22}{}^T=W_{f22}{}^T-\hat{W}_{f22}{}^T \tag{5.19c}$$

$$\tilde{W}_{f23}{}^T=W_{f23}{}^T-\hat{W}_{f23}{}^T \tag{5.19d}$$

If we choose weight matrix update rule as

$$\dot{\hat{W}}_2=-\Gamma_2\cdot\sigma_2(V^T\cdot h)\cdot\tilde{\tau}_{pr}+k_{p1}\cdot\Gamma_2\cdot\left\|\tilde{\tau}_{pr}\right\|\cdot\hat{W}_2 \tag{5.20a}$$

$$\dot{\hat{W}}_{f21}=-\Gamma_{f21}\cdot\varphi_{f21}(V_{f21}{}^T\cdot h)\cdot\tilde{\tau}_{pr}+k_{p1}\cdot\Gamma_{f21}\cdot\left\|\tilde{\tau}_{pr}\right\|\cdot\hat{W}_{f21} \tag{5.20b}$$

$$\dot{\hat{W}}_{f22}=-\Gamma_{f22}\cdot\varphi_{f22}[V_{f22}{}^T\cdot(h-v_s)]\cdot\tilde{\tau}_{pr}+k_{p1}\cdot\Gamma_{f22}\cdot\left\|\tilde{\tau}_{pr}\right\|\cdot\hat{W}_{f22} \tag{5.20c}$$

$$\dot{\hat{W}}_{f23}=-\Gamma_{f23}\cdot\varphi_{f23}[V_{f23}{}^T\cdot(h+v_s)]\cdot\tilde{\tau}_{pr}+k_{p1}\cdot\Gamma_{f23}\cdot\left\|\tilde{\tau}_{pr}\right\|\cdot\hat{W}_{f23} \tag{5.20d}$$

where $\Gamma_2=\Gamma_2{}^T>0$, $\Gamma_{f21}=\Gamma_{f21}{}^T>0$, $\Gamma_{f22}=\Gamma_{f22}{}^T>0$, $\Gamma_{f23}=\Gamma_{f21}3^T>0$ and k_{p1} is a positive constant

Define

$$\hat{\Theta}(h,v_s)=\hat{W}_2{}^T\cdot\sigma(V^T\cdot h)$$

$$+\hat{W}_{f21}{}^T\cdot\varphi_{22}(V_{f22}{}^T\cdot h)+\hat{W}_{f22}{}^T\cdot\varphi_{22}[V_{f22}{}^T\cdot(h-v_s)]+\hat{W}_{f23}{}^T\cdot\varphi_{23}[V_{f23}{}^T\cdot(h+v_s)] \tag{5.21}$$

And

$$\tilde{\Theta}(h,v_s)=\tilde{W}_2{}^T\cdot\sigma(V^T\cdot h)$$

$$+\tilde{W}_{f21}{}^{T}\cdot\varphi_{22}(V_{f22}{}^{T}\cdot h)+\tilde{W}_{f22}{}^{T}\cdot\varphi_{22}[V_{f22}{}^{T}\cdot(h-v_s)]+\tilde{W}_{f23}{}^{T}\cdot\varphi_{23}[V_{f23}{}^{T}\cdot(h+v_s)] \quad (5.22)$$

We get

$$\dot{\tilde{\tau}}_{pr}=-k_b\cdot\hat{\mu}\cdot K_a\cdot\tilde{\tau}_{pr}+(1-\hat{\mu}\cdot K_a)\cdot\dot{\tau}_{pd}+(1-\hat{\mu}\cdot K_a)\cdot\hat{\Theta}(h,v_s)+\tilde{\Theta}(h,v_s)+\varepsilon_2(h) \quad (5.23)$$

And the control rule Eq. (5.17) become

$$\dot{v}=\hat{\mu}\cdot[k_b\cdot\tilde{\tau}_{pr}+\dot{\tau}_{pd}+\hat{\Theta}(h,v_s)] \quad (5.24)$$

Design the update rule of estimator as

$$\dot{\hat{\mu}}=\Pr oj(\hat{\mu},\quad -\eta\cdot\tilde{\tau}_{pr}\cdot\hat{\mu}\cdot[\dot{\tau}_{pd}+\hat{\Theta}(h,v_s)]) \quad (5.25)$$

where η is positive constant. The $\Pr oj(\cdot)$ is a projection operator, which is defined as follows:

$$\dot{\hat{\mu}}=\Pr oj(\hat{\mu},\quad -\eta\cdot\tilde{\tau}_{pr}\cdot\hat{\mu}\cdot[\dot{\tau}_{pd}+\hat{\Theta}(h,v_s)]=$$

$$\begin{cases} 0 & if \quad \hat{\mu}=1 \quad and \quad \eta\cdot\tilde{\tau}_{pr}\cdot[\dot{\tau}_{pd}+\hat{\Theta}(h,v_s)]<0 \\ & if \quad \left(\dfrac{a_{\min}}{a_{\max}}\right)^2<\hat{\mu}<1 \\ -\eta\cdot\tilde{\tau}_{pr}\cdot\hat{\mu}\cdot[\dot{\tau}_{pd}+\hat{\Theta}(h,v_s)] & or \quad \hat{\mu}=1 \quad and \quad \eta\cdot\tilde{\tau}_{pr}\cdot[\dot{\tau}_{pd}+\hat{\Theta}(h,v_s)]\geq 0 \\ & or \quad \hat{\mu}=\left(\dfrac{a_{\min}}{a_{\max}}\right)^2 \quad and \quad \eta\cdot\tilde{\tau}_{pr}\cdot[\dot{\tau}_{pd}+\hat{\Theta}(h,v_s)]\leq 0 \\ 0 & if \quad \hat{\mu}=\left(\dfrac{a_{\min}}{a_{\max}}\right)^2 \quad and \quad \eta\cdot\tilde{\tau}_{pr}\cdot[\dot{\tau}_{pd}+\hat{\Theta}(h,v_s)]>0 \end{cases} \quad (5.26)$$

5.4 Composite adaptive controller and Hysteresis compensator

To provide precision control for piezoelectric actuator, we will integrate the hysteresis compensator with an adaptive robust controller.

For a piezoelectric actuator, the system dynamic model can be identified as a second-order linear model coupled with a hysteresis [38]

$$m \cdot \ddot{y}(t) + b \cdot \dot{y}(t) + k \cdot y(t) = k \cdot c \cdot \tau_{pd}(t) \tag{5.27a}$$

$$\tau_{pd}(t) = h[v(t)] \tag{5.27b}$$

where $y(t)$ denotes the position of piezoelectric actuator, m, b, k denote the mass, damping and stiffness coefficients. The hysteresis $h(t)$ is described by the Duhem model as Eq. (5.5).

Given a desired position of piezoelectric actuator $y_d(t) \in R^n$, which is continuous and its derivatives up to higher order are bounded, the tracking error of the piezoelectric actuator is defined as

$$e_p(t) = y_d(t) - y(t) \tag{5.28}$$

A filtered error is defined as

$$r_p(t) = \dot{e}_p(t) + \Lambda_p \cdot e_p(t) \tag{5.29}$$

where $\Lambda_p = \Lambda_p^{\ T} > 0$ a designed parameter matrix.

Differentiating $r_p(t)$ and combining it with the system dynamics Eq. (5.27a) and Eq. (5.27b), one may obtain:

$$\frac{m}{k \cdot c} \cdot \dot{r}_p = -\frac{b}{k \cdot c} \cdot r_p - \tau_{pd} + \frac{m}{k \cdot c} \cdot (\ddot{y}_d + \Lambda_p \cdot \dot{e}_p) + \frac{b}{k \cdot c} \cdot (\dot{y}_d + \Lambda_p \cdot e_p) + \frac{1}{c} \cdot y_d \tag{5.30}$$

The tracking error dynamics can be written in other form as

$$\frac{m}{k \cdot c} \cdot \dot{r}_p = -\frac{b}{k \cdot c} \cdot r_p - \tau_{pd} + Y_d^{\ T} \cdot \theta_p \tag{5.31}$$

where $Y_d = \left[\ddot{y}_d + \Lambda_p \cdot \dot{e}_p \quad \dot{y}_d + \Lambda_p \cdot e_p \quad y_d\right]^T$ as the input signal, and define

$\theta_p = \left[\frac{m}{k \cdot c} \quad \frac{b}{k \cdot c} \quad \frac{1}{c}\right]^T \in R^3$ and we have $\theta_{p\min} \le \theta_{pi} \le \theta_{p\max} \quad i = 1,2,3$ where $\theta_{p\min}$ and $\theta_{p\max}$ are some known real numbers.

Design the adaptive controller as

$$\tau_{pd} = -k_{pd} \cdot r_p + Y_d^T \cdot \hat{\theta}_p \tag{5.32}$$

The updating rule is designed as

$$\dot{\hat{\theta}}_p = \Pr oj_{\hat{\theta}_p}(\hat{\theta}_p, \quad -\beta \cdot Y_d \cdot r_p) \tag{5.33}$$

where β is positive constant adaptation rate diagonal matrix, $\beta = \phi \cdot e$ and

$$\{\Pr oj_{\hat{\theta}_p}(\hat{\theta}_p, \quad -\beta \cdot Y_d \cdot r_p)\}_i = \begin{cases} 0 & if \quad \hat{\theta}_{pi} = \theta_{p\max} \quad and \quad \beta \cdot (Y_d \cdot r_p)_i < 0 \\ & if \quad \theta_{p\min} < \hat{\theta}_{pi} < \theta_{p\max} \\ -\beta \cdot (Y_d \cdot r_p)_i & or \quad \hat{\theta}_{pi} = \theta_{p\max} \quad and \quad \beta \cdot (Y_d \cdot r_p)_i \ge 0 \\ & or \quad \hat{\theta}_{pi} = \theta_{p\min} \quad and \quad \beta \cdot (Y_d \cdot r_p)_i \le 0 \\ 0 & if \quad \hat{\theta}_{pi} = \theta_{p\min} \quad and \quad \beta \cdot (Y_d \cdot r_p)_i > 0 \end{cases} \tag{5.34}$$

Now, considering the piezoelectric actuator system with hysteresis nonlinearity. The overall control strategy of integrated controller is shown in Figure. 5-5

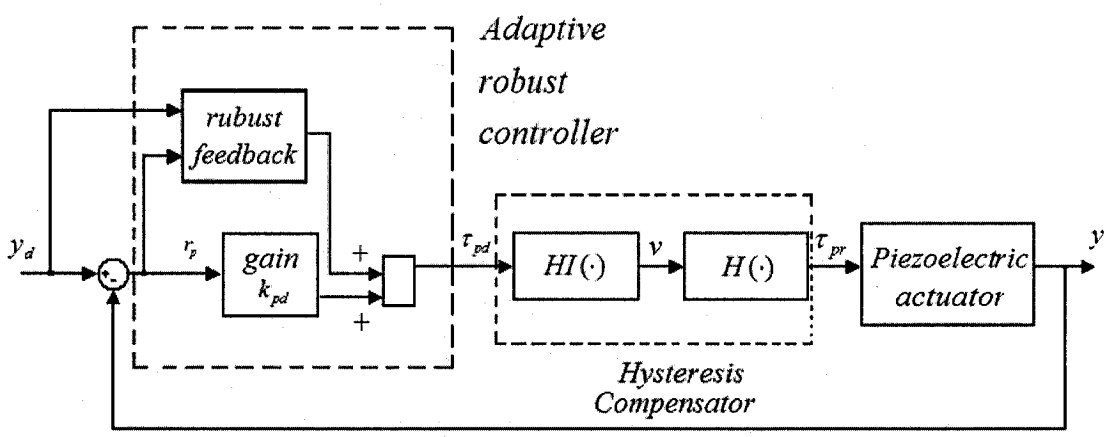

Figure 5-5 Adaptive robust controller with hysteresis compensator structure

Theorem 5.1

For a piezoelectric actuator system described by Eq. (5.27a) and Eq. (5.27b) with unknown hysteresis Eq. (5.1), with a desired trajectory $q_d(t)$, the system tracking error $e_p(t)$ is bounded with the adaptive robust controller and NN based compensator, which has the structure described in Eq. (5.32) and Eq. (5.24), respectively. The adaptive robust controller and the NN based compensator will tune following updating rule Eq (5.33), Eq (5.34) and Eq (5.18), Eq (5.25), Eq (5.26). Assume there exists sufficiently large compact set $\Omega_i \in R^{2i}$, $i=1,\ldots,n$ such that $Z_i \in \Omega_i$ for all $t \geq 0$. Then, the tracking error $e_p(t)$ will converge to a small neighbourhood around zero by appropriately choosing suitable gain matrix k_{pd} and k_b.

Proof

Define the Lyapunov function as

$$L_3 = \frac{1}{2}\cdot\frac{m}{k\cdot c}\cdot r_p^{\,2} + \frac{1}{2}\tilde{\tau}_{pr}^{\,2} + \frac{1}{2}\cdot tr(\tilde{\Theta}^T\Gamma_2^{-1}\tilde{\Theta}) + \frac{1}{2\cdot\eta}(\hat{\mu}-K_a)^2 + \frac{1}{2\beta}\cdot(\hat{\theta}_p-\theta_p)^T\cdot(\hat{\theta}_p-\theta_p) \tag{5.35}$$

We have $L_3 \geq 0' \frac{m}{k\cdot c}\cdot\dot{r}_p = -\frac{b}{k\cdot c}\cdot r_p - \tau_{pd} + Y_d^{\,T}\cdot\theta_p$. Differentiate Equation (5.35), yielding

$$\dot{L}_3 = \frac{m}{k\cdot c}\cdot r_p\cdot\dot{r}_p + \tilde{\tau}_{pr}\cdot\dot{\tilde{\tau}}_{pr} + tr(\tilde{\Theta}^T\Gamma_2^{-1}\dot{\tilde{\Theta}}) + \frac{1}{\eta}(\hat{\mu}-K_a)\cdot\dot{\hat{\mu}} + \frac{1}{\beta}\cdot(\hat{\theta}_p-\theta_p)^T\cdot\dot{\hat{\theta}}_p \tag{5.36}$$

Introducing control strategies Eq. (5.23), Eq. (5.32), and the update rule Eq. (5.33), Eq. (5.18), Eq. (5.25) into Lyapunov function Eq. (5.36), that is

$$\begin{aligned}\dot{L}_3 = & -\frac{b}{k\cdot c}\cdot r_p^{\,2} - \tau_{pd}\cdot r_p + Y_d^{\,T}\cdot\theta_p\cdot r_p \\ & + \tilde{\tau}_{pr}[-k_b\cdot\hat{\mu}\cdot K_a\cdot\tilde{\tau}_{pr} + (1-\hat{\mu}\cdot K_a)\cdot\dot{\tau}_{pd} + (1-\hat{\mu}\cdot K_a)\cdot\hat{\Theta} + \tilde{\Theta}] \\ & + tr(\tilde{\Theta}^T\cdot\Gamma_2^{-1}\cdot\dot{\tilde{\Theta}}) + \frac{1}{\eta}(\hat{\mu}-K_a)\cdot Proj(\hat{\mu}, \quad -\eta\cdot\tilde{\tau}_{pr}\cdot\hat{\mu}\cdot[\dot{\tau}_{pd} + \hat{W}_2^{\,T}\cdot\sigma(V^T\cdot h)]) \\ & + \frac{1}{\beta}\cdot(\hat{\theta}_p-\theta_p)^T\cdot Proj_{\hat{\theta}_p}(\hat{\theta}_p, \quad -\beta\cdot Y_d\cdot r_p)\end{aligned} \tag{5.37}$$

From updating rule Eq (5.26), and Eq (5.34) we get

$$\begin{aligned}& \frac{1}{\eta}(\hat{\mu}-K_a)\cdot Proj(\hat{\mu}, \quad -\eta\cdot\tilde{\tau}_{pr}\cdot\hat{\mu}\cdot[\dot{\tau}_{pd} + \hat{\Theta}]) \\ & \leq -\tilde{\tau}\cdot(\hat{\mu}^2 - \hat{\mu}\cdot K_a)\cdot\dot{\tau}_d\cdot\omega - \tilde{\tau}\cdot(\hat{\mu}^2 - \hat{\mu}\cdot K_a)\cdot\hat{\Theta} \\ & \leq -\tilde{\tau}\cdot(1-\hat{\mu}\cdot K_a)\cdot\dot{\tau}_d\cdot\omega - \tilde{\tau}\cdot(1-\hat{\mu}\cdot K_a)\cdot\hat{\Theta}\end{aligned}$$

$$\frac{1}{\beta}\cdot(\hat{\theta}_p-\theta_p)^T\cdot Proj_{\hat{\theta}_p}(\hat{\theta}_p, \quad -\beta\cdot Y_d\cdot r_p) \leq -\beta\cdot(\hat{\theta}_p-\theta_p)^T\cdot Y_d\cdot r_p$$

So, we have

$$\dot{L}_2 \le -(\frac{b}{k \cdot c} + k_{pd}) \cdot r_p{}^2 - k_b \cdot \hat{\mu} \cdot K_a \cdot \left\|\tilde{\tau}_{pr}\right\|^2 + \left\|\tilde{\tau}_{pr}\right\| \cdot \varepsilon_N - k_{p1} \cdot \left\|\tilde{\tau}_{pr}\right\| tr(\tilde{\Theta}^T \hat{\Theta}) \tag{5.38}$$

$$\le -(\frac{b}{k \cdot c} + k_{pd}) \cdot r_p{}^2 - K_b \cdot \left\|\tilde{\tau}_{pr}\right\|^2 + \left\|\tilde{\tau}_{pr}\right\| \cdot \varepsilon_N - k_{p1} \cdot \left\|\tilde{\tau}_{pr}\right\| \cdot \left\|\tilde{\Theta}\right\| (\Theta_N - \left\|\tilde{\Theta}\right\|) \tag{5.39}$$

where $K_b = k_b \cdot a_{\max}$ and $\Theta_N = W_{2N} + W_{f21N} + W_{f22N} + W_{f23N}$

If we have

$$\left\|\tilde{\tau}\right\| > \frac{k_{p1} \cdot \Theta_N{}^2 / 4 - \varepsilon_N}{K_b} \tag{5.40}$$

Or

$$\left\|\tilde{W}_2\right\| > W_N / 2 + \sqrt{W_N{}^2 / 4 + \varepsilon_N / k_{p1}} \tag{5.41}$$

We can prove $\dot{L}_3$ negative. Inequality (5.41) shows that if the control gain k_{pd} and k_b is chosen large enough so that

$$\frac{k_{p1} \cdot \Theta_N{}^2 / 4 - \varepsilon_N}{K_b} < b_r \tag{5.42}$$

where $b_r > 0$ represents the radius of a ball inside the compact set C_r of filtered error $\tilde{\tau}_{pr}(t)$.

Thus, any trajectory $y_d(t)$ starting in compact set $C_r = \{r \mid \|r\| \le b_r\}$ converges within C_r and is bounded. Then filtered error of system $r_p(t)$ and the tracking error of the hysteresis $\tilde{\tau}_{pr}(t)$ converges to a small neighbourhood around zero. According to the standard Lyapunov theorem extension [45], this demonstrates the UUB (uniformly ultimately bounded) of $r_p(t)$, $\tilde{\tau}_{pr}(t)$ and $\tilde{\Theta}$.

5.5 Conclusion

In the proposed adaptive NN compensator for unknown hysteresis, an augmented feedforward MLP are used to approximate a complicated piecewise continuous unknown nonlinear functions. No off-line training is required for the NN. The control algorithm and the weight matrix update rule are derived from Lyapunov theorem extension. With the designed adaptive controller for piezoelectric actuator, the stability of the integrated system and the boundedness of tracking error of the piezoelectric actuator with unknown hysteresis have been proved. Simulation results in chapter 6 show the effectiveness of the proposed NN compensator in detail.

Chapter 6 Simulation results

In this chapter, the effectiveness of the hysteresis compensator is demonstrated on a piezoelectric actuator described by Eq (5.27) with unknown hysteresis.

The coefficients of the dynamic system and hysteresis model are identified in Table 6-1.

Table 6-1 coefficients of the piezoelectric actuator and hysteresis model

System Parameters	Values
m (mass coefficient)	0.016
b (damping coefficient)	1.2
k (stiffness coefficient)	4500
c	0.9
a_1	6
a_2	2
a_3	0.5
v_s	6

6.1 Control Performance of Hysteresis Compensator

Assuming piezoelectric actuator works without the hysteresis and controlled by the proposed adaptive controller. Two input reference signal are chosen as desired two joints positions: $y_{1d} = 2 \cdot \sin(0.1\pi \cdot t)$ and $y_{2d} = 3 \cdot \sin(0.1\pi \cdot t)$. The control objective is defined as to make the output signal $y = [y_1 \quad y_2]^T$ follow the given desired

trajectory $y_d = [y_{1d} \quad y_{2d}]^T$. The gains of system controller are selected as: $\beta = diag\{0.1 \quad 0.1\}$, $k_{pd} = diag\{50 \quad 50\}$. The system responses under the control of the adaptive controller are shown in Fig. 6-1.

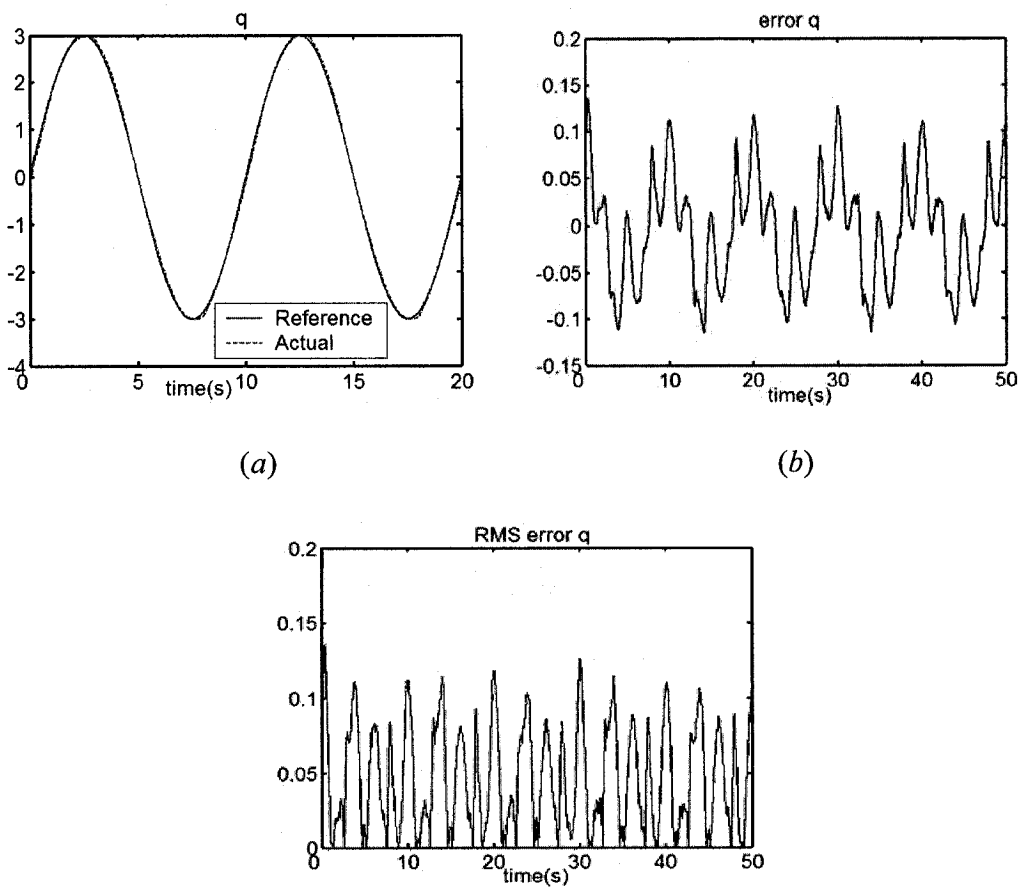

(*a*) (*b*)

(*c*)

Figure 6-1 Performance of NN controller without hysteresis

(a) The actual control signal (dashed line) with reference (solid) control signal

(b) Error $q - q_d$ (c) RMS Error $q - q_d$

The responses of the same system with hysteresis but no compensator are shown in

Fig. 6-2. In which, the gains of system controller are selected as: $\beta = diag\{0.1 \quad 0.1\}$, $k_{pd} = diag\{50 \quad 50\}$.

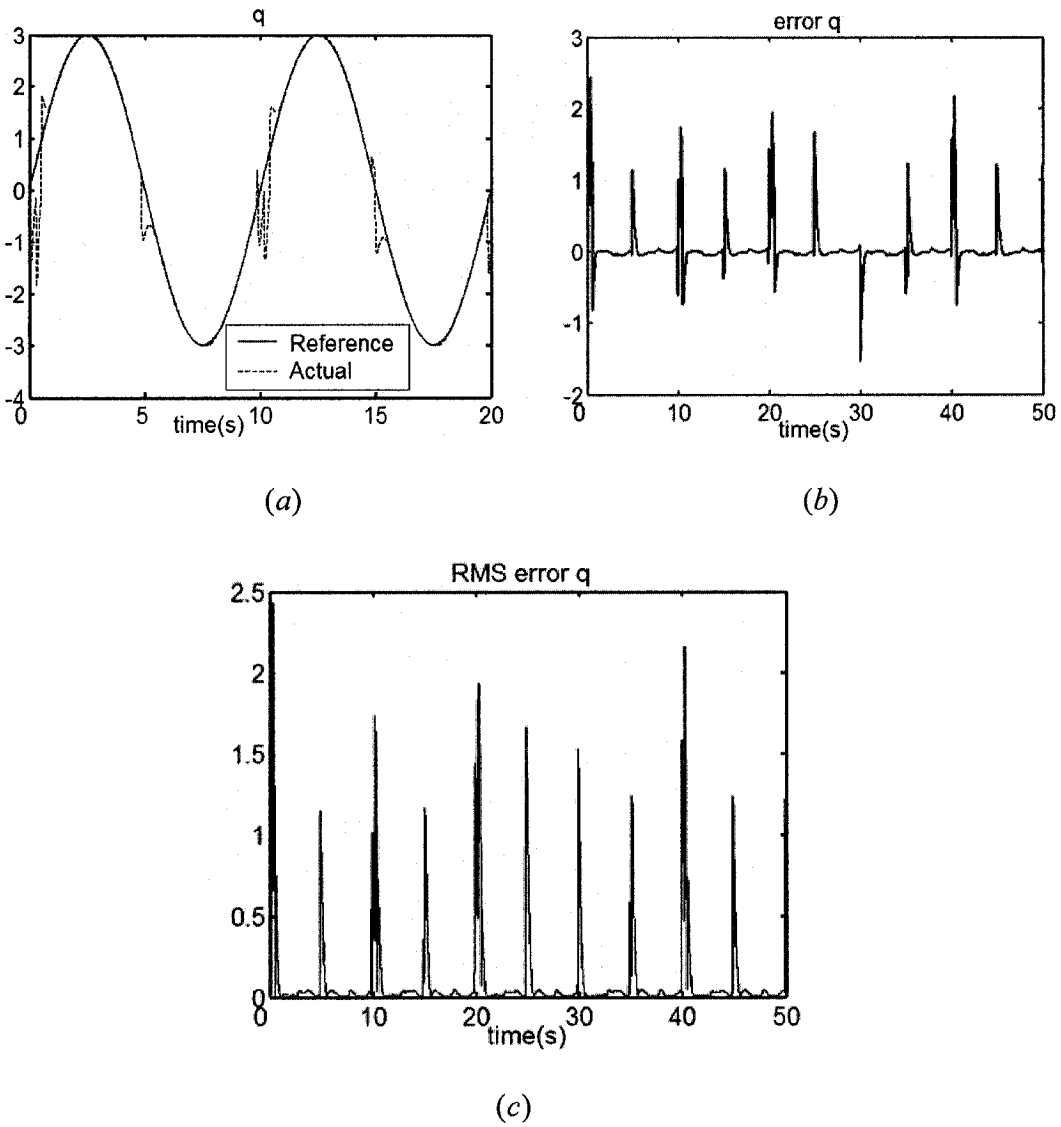

(*a*) (*b*)

(*c*)

Figure 6-2 Performance of NN controller with hysteresis but without compensator

(a) The actual control signal (dashed line) with reference (solid) control signal

(b) Error $q - q_d$ (c) RMS Error $q - q_d$

The responses of the same system with hysteresis and hysteresis compensator are shown in Fig. 6-3. In which, the gains of system controller are selected as: $\beta = diag\{0.1 \quad 0.1\}$, $k_{pd} = diag\{50 \quad 50\}$. The gains of hysteresis compensator are selected as: $K_a = diag\{20 \quad 20\}$, $k_b = diag\{100 \quad 100\}$, $\Gamma_2 = \Gamma_{f21} = \Gamma_{f22} = \Gamma_{f23} = diag\{10 \quad 10\}$, and $\eta = diag\{0.1 \quad 0.1\}$.

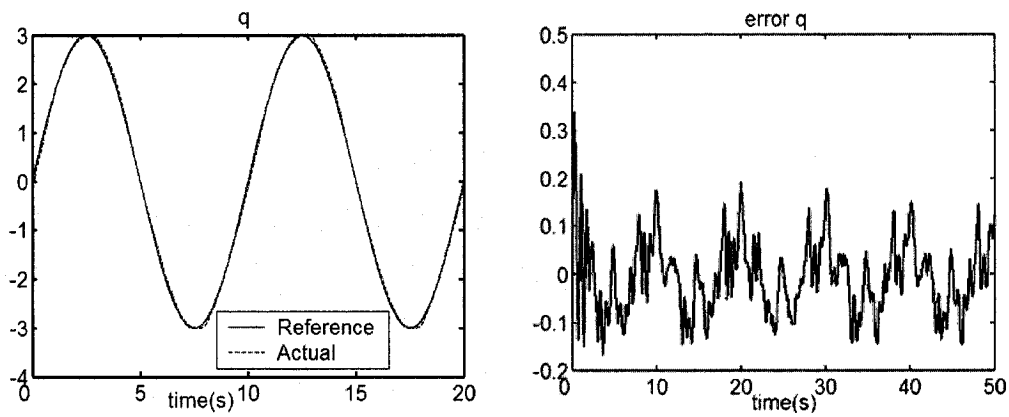

(*a*) (*b*)

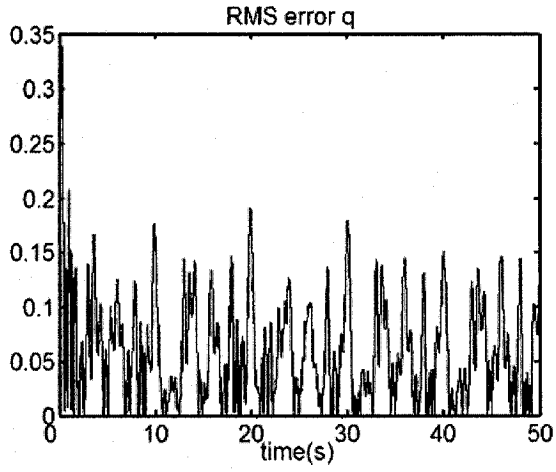

(*c*)

Figure 6-3 Performance of NN controller with hysteresis and hysteresis compensator

(a) The actual control signal (dashed line) with reference (solid) control signal

(b) Error $q - q_d$ (c) RMS Error $q - q_d$

The compensator's input and output curve, the hysteresis's input and output curve, and the desired control signal and real control signal curve are given in Fig. 6-4.

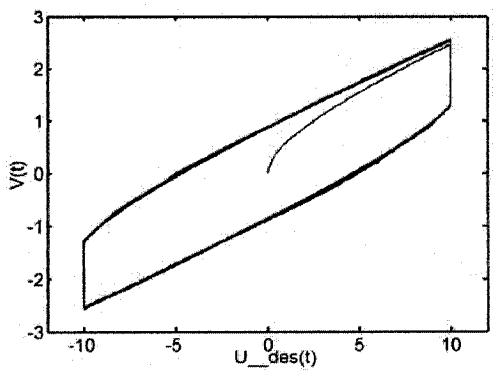

(a)

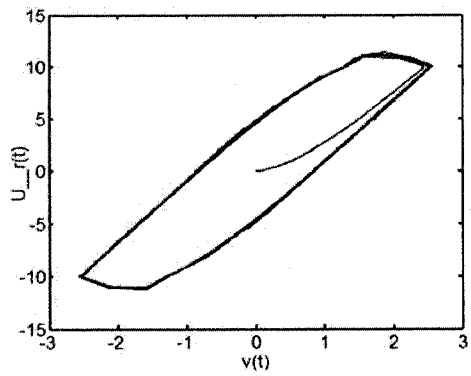

(b)

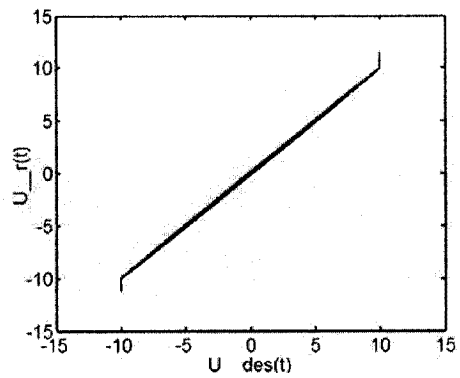

(c)

Figure 6-4 Performance of NN controller with hysteresis and hysteresis compensator

The compensator's input signal $u_{des}(t)$ and output signal $v(t)$ curve

The hysteresis's input signal $v(t)$ and output signal $u_r(t)$ curve

The desired control signal $u_{des}(t)$ and real control signal $u_r(t)$ curve

6.2 Conclusion

Fig. 6-1--6-4 shows the simulation results of applying the hysteresis compensator to piezoelectric actuator system with unknown hysteresis for tracking a desired signal. We can see that a very good tracking performance is obtained. The NN based compensator can indeed improve the tracking performance by cancel the effect of hysteresis. In addition, it is a significant advantage since the NN compensator can be applied to any type of system dynamics to remove the hysteresis phenomena.

Chapter 7 Conclusions and Future work

In the thesis, adaptive neural network (NN) controllers for a Rigid Link Flexible Joint (RLFJ) robot manipulator with unknown nonlinearities have been proposed. A two link RLFJ robot is studied using the proposed control schemes. The simulation results reveal that the presented NN controller can indeed improve the tracking performance without resorting to high-gain feedback. In addition, we do not even need to know the explicit parameters of system. Moreover, the NN controller can be implemented in a wide stiffness parameter range. This is a significant advantage since the NN controller can be applied to many type of flexible or rigid robots with little modification to gain parameters.

A piezoelectric actuator is also studied for the application of NN based hysteresis compensator. The simulation results reveal that the proposed NN compensator achieves good tracking precision with stabilization with parameter uncertainty. The compensator is design separately for removing the effect of hysteresis phenomena. Hence, it can work with other controller in various nonlinear systems proceeding with hysteresis.

The main contributions of this research are summarized as:

1) In RLFJ controller design, two NNs are utilized to alleviate the symbolic computational burden by approximating two complicated nonlinear function of both fast subsystem and slow subsystem.
2) A fictitious variable is introduced in the design of adaptive NN controller to provide sufficient damping for the fast dynamics when dealing with joint elasticity in fast subsystem.

3) An augmented NN is used to approach a piecewise continuous nonlinear function in hysteresis compensator design.
4) An NN based inverse hysteresis compensator is developed to cancel the hysteresis effect.
5) The hysteresis compensator is used in a piezoelectric actuator with an adaptive controller to track the desired trajectory.
6) All the NNs developed in both RLFJ robot manipulator control and piezoelectric actuator with the hysteresis are turned on-line. No offline trainings are needed.
7) The system stability, boundedness of tracking errors and NN weight matrix in both RLFJ robot manipulator control and piezoelectric actuator with the hysteresis are guaranteed by Lyapunov theorem extension.

Possible future works are list as follows:

1) Due to the potential benefits to space robot and industrial applications, the demands of flexible link robot manipulators are increased. The possible next step research is to take the Link elasticity into account in these flexible link robot manipulators.
2) In order to operate in real-time with high precision, the payload is an extremely important issue for industrial application. The further research will be the investigation for NN based control strategy with respect to a time varying payload at the end of a robot manipulator.
3) Some assumptions are made for the hysteresis Duhem model during the hysteresis compensator design. The NN based inverse hysteresis compensator for general Duhem model and other hysteresis model will be the further

research area.

4) This actual control signal of piezoelectric actuator is needed for the proper work of NN based inverse hysteresis compensator. In reality, this signal is difficult to measure. The possible next step research is to remove the necessity of this signal.

References

[1] R. Horowitz and M. Tomizuka, *"An adaptive control scheme for mechanical manipulators – compensation of nonlinearity and decoupling control,"* ASME Journal of Dynamic Systems Measurement and Control, vol. 108, no. 2, pp.127-135, 1986.

[2] S. Nicosia and P. Tomei, *"Robot Control by using only Joint Position Measurement,"* IEEE Transactions on Automatic Control, vol. 35, no. 9, pp.1058-1061, 1990.

[3] J. J. Craig, P. Hsu, and S. S. Sastry, *"Adaptive Control of Mechanical Manipulators,"* Proceedings of the IEEE International Conference on Robotics and Automation, pp. 190-195, San Francisco, CA, 1986.

[4] J. J. E. Slotine and W. Li, *"Adaptive Manipulator Control: a case study,"* IEEE Transactions on Automatic Control, vol. 33, no. 11, pp. 995-1003, Nov. 1988.

[5]. M.W. Spong, *"Modeling and Control of Elastic Joint Manipulators,"* Journal of Dynamic Systems, Measurement and Control, Vol. 109, pp.310-319, 1987.

[6] A. De Luca, *"Decoupling and Feedback Linearization of Robots with Mixed Rigid/Flexible Joint Robots,"* Proceedings of the IEEE International Conference on Robotics and Automation, pp.1115-1120, 1996.

[7] M. W. Spong *"Adaptive Control of Flexible Joint Manipulators,"* Systems and Controls Letters, vol. 13, no. 1, pp. 15-21, 1989.

[8] O. Aboulshamat and P. Sicard *"Position Control of A Flexible Joint with Friction Using Neural Network Feedforward Inverse Models,"* Proceeding of the Canadian Conference on Electrical and Computer Engineering, pp. 283-388, Toronto, Canada, 2001.

[9] F. Abdollahi, H. A. Talebi, and R.V. Patel, *"State Estimation for Flexible-Joint Manipulators using Stable Neural Networks,"* Proceeding of the IEEE International Symposium on Computation Intelligence in Robotics and Automation, pp. 25-29, Kobe, Japan, 2003.

[10] W.H. Zhu and J. De Schutter, *"Adaptive Control of Mixed Rigid/Flexible Joint Robot Manipulators Based on Virtual Decomposition,"* IEEE Transactions on Robotics and Automation, Vol. 5, No.2, pp 310-317, April 1999.

[11] C. Kwan, F. L. Lewis, and D. M. Dawson, *"Robust Neural-Network Control of Rigid-Link Electrically Driven Robots,"* IEEE Transactions on Neural Networks, vol. 9, no. 4, pp.581-588, 1998.

[12] D. Shukla, D. M. Dawson, and F. W. Paul, *"Multiple Neural-Network-Based*

Adaptive Controller Using Orthonormal Activation Function Neural Networks," IEEE Transactions on Neural Networks, vol. 10, no. 6, pp.1494-1501, 1999.

[13]. C. M. Kwan, F. L. Lewis, and Y. H. Kim, *"Robust Neural Network control of rigid link flexible-joint robots,"* Asian Journal Of Control, vol. 1, no. 3, pp. 188-197, 1999.

[14] S. S. Ge and C. Wang, *"Direct Adaptive NN Control of a Class of Nonlinear System,"* IEEE Transactions on Neural Networks, Vol. 13, No. 1, pp.214-221, 2002.

[15] Joong-Seok Moon, W. C. Athas, and P.A Beerel, *"Theory and practical implementation of harmonic resonant rail driver,"* Low Power Electronics and Design, International Symposium, pp. 153 – 158, Aug 2001.

[16] H. Kohorramabadi, J. Anidjar, and T.R. Peterson, *"A highly efficient CMOS line driver with 80-dB linearity for ISDN U-interface applications,"* IEEE Journal of Solid-State Circuits, Vol. 29, No. 7, pp. 844 – 850, July 1994.

[17] S. Cetinkunt and W. J. Book, *"Performance limitations of joint variable feedback controllers due to manipulator flexibility,"* IEEE Transactions on Robots and Automation, vol. 6, pp.219-231, April 1990.

[18] R. Lozano and B. Brogliato, *"Adaptive Control of Robot Manipulators with Flexible Joint,"* IEEE Transactions on Automatic Control, vol. 37, no. 2, pp. 174-181, February

1990.

[19] R. F. Jacobus, and M. A. Serna, *"Modal analysis of a three dimensional flexible robot,"* Proceedings of the IEEE International Conference on Robotics and Automation, Vol. 4, pp. 2962 – 2967, May 1994.

[20] A. Garcia, and V. Feliu, *"Force control of a single-link flexible robot based on a collision detection mechanism,"* Proceedings of the IEEE International Conference on Control Theory and Applications, Vol. 147, pp. 588 –595, November 2000.

[21] R. A. Al-Ashoor, R. V. Patel, and K. Khorasani, *"Robust Adaptive Controller Design and Stability Analysis for Flexible-Joint Manipulators,"* IEEE transactions on Systems, Man and Cybernectics, vol. 23, no. 2, pp.589-602, 1993.

[22] F. Ghorbel, J. Y. Hung, and M. W. Spong, *"Adaptive Control of Flexible-Joint Manipulators,"* IEEE Control System Magazine, vol. 9, no. 7, pp. 9-13, 1989.

[23] F. Ghorbel and M. W. Spong, *"Adaptive Integral Manifold Control of Flexible Joint Manipulators,"* Proceedings of the IEEE International Conference on Robotics and Automation, pp.707-714, Nice, France, 1992

[24] M. Moallem, K. Khorasani, and R. V. Patel, *"An Integral Manifold Approach for Tip-Position Tracking of Flexible Multi-Link Manipulators,"* IEEE Transactions on

Robotics and Automation, vol. 13, no. 6, pp. 823-837, 1997.

[25] F. Ghorbel and M. W. Spong, *"Adaptive Integral Manifold Control of Flexible Joint Manipulators,"* Proceedings of the IEEE International Conference on Robotics and Automation, pp.707-714, Nice, France, 1992

[26] J. De Leon-Morales, R. Castro-Linares, Ja. Alvarez-Gallegos, and J. M. Mendivil-Avila, *"Controller-Observer Scheme for a Class of Nonlinear Singularly Perturbed Systems,"* Proceedings of the 40th IEEE Conference on Desision and Control, pp.1372-1377, Orlando, FL, 2001.

[27] F. L. Lewis, Aydin Yesildirek, and Kai Liu, *"Multilayer Neural-Net Robot Controller with Guaranteed Tracking Performance,"* IEEE transactions on Neural Network, vol. 7, no. 2, pp.388-398, March 1996.

[28] V. Zeman, R.V. Patel, and K. Khorasani, *"Control of a Flexible-Joint Robot Using Neural Networks,"* IEEE Transactions on Control Systems Technology, Vol. 5, No. 4, pp.453-462, 1997

[29] W. Chatlatanagulchai and P. H. Mechl, *"Motion Control of Two-Link Flexible-Joint Robot, Using Backstepping, Neural Networks and Indirect Method,"* Proceeding of the IEEE International Conference on Control Applications, pp. 601-605, Toronto, Canada, 2005.

[30] Lianfang Tian, Jun Wang, and Zongyuan Mao, *"Constrained Motion Control of Flexible Robot Manipulators Based on Recurrent Neural Networks,"* IEEE Transactions on Systems, Man, and Cybernetics, part B: Cybernetics, vol. 34, no. 3, June 2004.

[31] D. C. Jiles, and D. L. Atherton, *"Theory of ferromagnetic hysteresis,"* J. Magnet. Magn. Mater., vol. 61, pp. 48-60, 1986

[32] Ram Venkataraman Iyer, Xiaobo Tan, and P. S. Krishnaprasad, *"Approximate Inversion of the Preisach Hysteresis Operator With Application to Control of Smart Actuators,"* IEEE Transactions on Automatic Control, vol. 50, no. 6, June 2006.

[33] Xiaobo Tan, and John S. Baras, *"Adaptive Identification and Control of Hysteresis in Smart Materials,"* IEEE Transactions on Automatic Control, vol. 50, no. 6, June 2006.

[34] F. Alija Garmon, W. T. Ang, P. K. Khosla, and C. N. Riviere, *"Rate-Dependent Inverse Hysteresis Feedforward Controller for Microsurgical Tool,"* Proceedings of the 25th Annual International Conference of the IEEE EMBS, pp.3415-3418, Cancun, Mexico, September 2003.

[35] Chun-Yi Su, Qingqing Wang, Xinkai Chen, and Subhash Rakheja, *"Adaptive Variable Structure Control of a Class of Nonlinear Systems with Unknown Prandtl-Ishlinskii Hysteresis,"* IEEE Transactions on Automatic Control, vol. 50, no. 12,

December 2005.

[36] Natale C., Velardi F., and Visone C., *"Modelling and compensation of hysteresis for magnetostrictive actuators,"* Proceedings of the IEEE/ASME International Conference on Advanced Intelligent Mechatronics, pp.744-749, 2001.

[37] Gang Tao, and Petar V. Kokotovic, *"Adaptive control of Plants with Unknown Hysteresis,"* IEEE Transactions on Automatic Control, vol. 40, no. 2, February 1995

[38] Chau Jan, and Chih-Lyang Hwang, *"Robust Control Design for a Piezoelectric Actuator System with Dominant Hysteresis, "* Industrial Electronics Society, 2000. IECON 2000, 26th Annual Conference of the IEEE, vol. 3, pp. 1515-1520, October 2000

[39] Dimitre Makaveev, Luc Dupre, and Jan Melkebeek, *"Neural-Network-Based Approach to Dynamic Hysteresis for Circular and Elliptical Magnetization in Electrical Steel Sheet,"* IEEE Transactions on Magnetics, vol. 38, no. 5, September 2002.

[40] M. Kuczmann, and A. Ivanyi, *"A New Neural-Network-Based Scalar Hysteresis Model,"* IEEE Transactions on Magnetics, vol. 38, no. 2, March 2002.

[41] M. Beuschel, F. Hangl, and D. Schroder, *"A General Approach for Hysteresis Modeling and Identification Using Neural Networks,"* Neural Networks Proceeding of the 1998 IEEE world Congress on Computational Intelligence. The 1998 IEEE

International Joint Confercence, vol. 3, 4-9 May 1998

[42] Xing-Song, Wang. Li Li, Chun-Yi Su and Henry Hong, *"Recurrent Neural Network Control of Dynamic Systems with Unknown Input Hysteresis,"* Proceedings of the IEEE International Conference on Neural Networks and Signal Processing, pp.297-300, Nanjing, China, 2003

[43] Visone C., Serpicob C., Mayergoyzb J. D., Huangb M. W., and Adly A. A., *"Neural Preisach type Models and their Application to the Identification of Magnetic Hysteresis from Noisy Data,"* Physica B275. pp. 223-227, 2000.

[44] Chun-Yi Su, Yury Stepanenko, Jaroslav Svoboda, and T. P. Leung, *"Robust Adaptive Control of a Class of Nonlinear Systems with Unknown Backlash-Like Hysteresis,"* IEEE Transactions on Automatic Control, vol. 45, no. 12, December 2000.

[45] K. S. Narendra and A. M. Annaswamy, *Stable Adaptive Systems,* Englewood Cliffs, New Jersey: Prentice Hall, 1989

[46] N. K. Bose, and P. Liang, "*Neural Network Fundamentals with Graphs, Algorithms, and Applications.*" New Delhi, India: Tada, McGraw-Hill, 1998

[47] S. Haykin, "*Neural Networks: A Comprehensive Foundation.*" NJ, Prentice-Hal, 1999

[48] F. M. Ham, and I. Kostanic, "*Principles of Neurcomputing for Science and Engineering*." Singapore, McGraw-Hill, 2001

[49] K. Hornik, M. Stinchcombe, et al, "*Multilayer feedforward networks are universal approximators*." Neural Networks 2: 359-366, 1989

[50] K. Hornik, M. Stinchombe and H. White, *"Multilayer Feedforward Networks are Universal Approximators,"* Neural Networks, vol. 2, pp. 359-366, 1989

[51] J. Park, and I. W. Sandberg, *"Universal Approximation Using Radial-Basis-Function Networks,"* Neural Computation, vol. 3, pp. 246-257, 1991

[52] R. M. Sanner, and J. J. E. Slotine, *"Stable Adaptive Control via Neural Networks,"* Proceedings of the IEEE International Conference on Decision and Control, 1991

[53] R. R. Selmic, and F. L. Lewis, *"Deadzone Compensation in Motion Control Systems Using Dynamical Neural Networks,"* IEEE Transactions on Automatic Control, vol. 45, no. 4, April 2000.

[54] R. R. Selmic, and F. L. Lewis, *"Neural Network Approximation of Piecewise Continuou Functions: Application to Friction Compensation,"* IEEE Transactions on Neural Networks, vol. 13, no. 3, May 2002.

[55] P. Lischinsky, C. Canudas-de-Wit and G. Morel, *"Friction Compensation for an Industrial Hydraulic Robot,"* Control Systems Magazine. IEEE, vol. 19, pp. 25-32, February 1999.

[56] C. Canudas de Wit, H. Olsson, K. J. Astrom, and P. Lischinsky, *"A New Model for Control of Systems with Friction,"* IEEE Transactions on Automatic Control, vol. 40, no. 3, pp. 419-425, March 1995.

[57] Marion, J. B., *Classical Dynamics.* New York: Academic Press, 1965.

[58] JinHyoung Oh, and Dennis S. Bernstein, *"Semilinear Duhem Model for Rate-Independent and Rate-Dependent Hysteresis,"* IEEE Transactions on Automatic Control, vol. 50, no. 5, May 2005.

[59] Ashwani K. Padthe, JinHyoung Oh, and Dennis S. Bernstein, *"Counterclockwise Dynamics of Rate-Independent Semilinear Duhem Model,"* Proceeding of the 44th IEEE Conference on Decision and Control, and the European Control Conference 2005, Seville, Spain, December 2001

[60] Han. Yao, W. F. Xie, and Cang Ye, *"A Composite Approach to the Adaptive Neural Networks Control of Unknown Flexible Joint Robots,"* International Conference on Dynamics, Instrumentation and Control, Queretaro, Mexico, August 2006.